Ancient TL

www.ancienttl.org · ISSN: 2693-0935

Issue 36(1) - June 2018
https://doi.org/10.26034/la.atl.v36.i1

This issue is published under a Creative Commons Attribution 4.0 International (CC BY):
https://creativecommons.org/licenses/by/4.0

© Ancient TL, 2018

ISSN 0735-1348

Ancient TL

A periodical devoted to Luminescence and ESR dating

Department of Physics, East Carolina University, 1000 East 5th Street, Greenville, NC 27858, USA
http://ancienttl.org

June 2018, Volume 36 No.1

Quantifying hydrofluoric acid etching of quartz and feldspar coarse grains based on weight loss estimates: implication for ESR and luminescence dating studies 1
M. Duval, V. Guilarte, I. Campaña, L.J. Arnold, L. Miguens, J. Iglesias, S. González-Sierra

Thesis abstracts 15

Bibliography 18

Announcements 32

Ancient TL

Started by the late David Zimmerman in 1977

EDITOR

Regina DeWitt, Department of Physics, East Carolina University, Howell Science Complex, 1000 E. 5th Street Greenville, NC 27858, USA; Tel: +252-328-4980; Fax: +252-328-0753 (dewittr@ecu.edu)

EDITORIAL BOARD

Ian K. Bailiff, Luminescence Dating Laboratory, Univ. of Durham, Durham, UK (ian.bailiff@durham.ac.uk)
Geoff A.T. Duller, Institute of Geography and Earth Sciences, Aberystwyth University, Ceredigion, Wales, UK (ggd@aber.ac.uk)
Sheng-Hua Li, Department of Earth Sciences, The University of Hong Kong, Hong Kong, China (shli@hku.hk)
Shannon Mahan, U.S. Geological Survey, Denver Federal Center, Denver, CO, USA (smahan@usgs.gov)
Richard G. Roberts, School of Earth and Environmental Sciences, University of Wollongong, Australia (rgrob@uow.edu.au)

REVIEWERS PANEL

Richard M. Bailey
Oxford, UK
richard.bailey@ouce.ox.ac.uk

James Feathers
Seattle, WA, USA
jimf@uw.edu

Rainer Grün
Canberra, Australia
rainer.grun@anu.edu.au

David J. Huntley
Burnaby B.C., Canada
huntley@sfu.ca

Sebastian Kreutzer
Bordeaux, France
sebastian.kreutzer@u-bordeaux-montaigne.fr

Michel Lamothe
Montréal, Québec, Canada
lamothe.michel@uqam.ca

Norbert Mercier
Bordeaux, France
norbert.mercier@u-bordeaux-montaigne.fr

Didier Miallier
Aubière, France
miallier@clermont.in2p3.fr

Andrew S. Murray
Roskilde, Denmark
anmu@dtu.dk

Vasilis Pagonis
Westminster, MD, USA
vpagonis@mcdaniel.edu

Naomi Porat
Jerusalem, Israel
naomi.porat@gsi.gov.il

Daniel Richter
Leipzig, Germany
drichter@eva.mpg.de

David C.W. Sanderson
East Kilbride, UK
David.Sanderson@glasgow.ac.uk

Andre Sawakuchi
São Paulo, SP, Brazil
andreos@usp.br

Ashok K. Singhvi
Ahmedabad, India
singhvi@prl.res.in

Kristina J. Thomsen
Roskilde, Denmark
krth@dtu.dk

Web coordinators: Joel DeWitt, Regina DeWitt
Article layout and typesetting: Regina DeWitt
Bibliography: Sebastien Huot

Ancient TL

Quantifying hydrofluoric acid etching of quartz and feldspar coarse grains based on weight loss estimates: implication for ESR and luminescence dating studies

M. Duval[1,2*], V. Guilarte[3], I. Campaña[2], L.J. Arnold[4], L. Miguens[2], J. Iglesias[2], S. González-Sierra[5]

[1] Australian Research Centre for Human Evolution (ARCHE), Environmental futures Research Institute Griffith University, Nathan QLD 4111, Australia

[2] Centro Nacional de Investigación sobre la Evolución Humana, Paseo de Atapuerca, 3, 09002 Burgos, Spain

[3] Departamento de Didáctica de las Ciencias Experimentales. Facultad de Educación y Humanidades de Melilla Universidad de Granada, Spain

[4] School of Physical Sciences, Institute for Photonics and Advanced Sensing (IPAS) and Environment Institute University of Adelaide, North Terrace Campus, Adelaide, SA 5005, Australia

[5] Max Planck Institute for Terrestrial Microbiology, Karl-von-Frisch-Strasse 16, 35043 Marburg, Germany

*Corresponding Author: m.duval@griffith.edu.au

Received: April 19, 2018; in final form: April 20, 2018

Abstract

A series of hydrofluoric (HF) acid etching experiments were performed on several 50 to 300 μm (nominal sieve opening) quartz and feldspar samples, and average etching thicknesses were subsequently determined from weight loss estimates, following the approach of Bell & Zimmerman (1978). Our results are consistent with previous studies and confirm that both HF experimental conditions (etching time, HF concentration, agitation) and the nature/origin of the minerals have a significant effect on etching rate and magnitude. For the samples considered in this study, the outer 10 μm of quartz (i.e., the usual etching target in most ESR and luminescence dating studies) was removed with 40% HF after 40 min of etching, in fair agreement with previous studies. Similar etching results were achieved in just over 20 min when the quartz samples were constantly agitated during 40% HF treatment. For K-feldspars, 10% HF etching for between 10 and 40 min was required to remove the same thickness, although some variability in etching efficiency was evident between different samples and experimental conditions. For a given experimental setup, the overall variability in etching thickness among quartz samples was found to be of at least 20% after 40–60 min with 40% HF, and can be as high as ∼35%. A set of 14 K-feldspars from a single site revealed an inherent variability of 14% in etching thickness. As a first order approximation, these data may provide useful insights into the expected variability among samples of different origin and from a given area, respectively. However, we recommend that each laboratory evaluates etching thickness losses for their specific HF experimental setup. Additionally, our results show that the 10 μm etching usually considered in ESR and luminescence dating studies may reduce the alpha contribution of the total dose rate to <5%. Although relatively small, this contribution is nevertheless non-negligible. Based on these results, it may be worth considering an additional alpha dose rate term as part of the ESR and luminescence age calculation when etching depths are < 15 μm.

Keywords: hydrofluoric acid (HF); etching; Luminescence dating; ESR dating; Quartz; Feldspar; weight loss

1. Introduction

Quantifying the effects of hydrofluoric acid (HF) etching on quartz and feldspar grains is crucial for both Electron Spin Resonance (ESR) and luminescence dating applications. An estimate of the outer thickness removed from silicate grains by HF etching is needed for accurate evaluation of both the internal and external alpha and beta dose rate components (see Aitken, 1985). However, obtaining reliable etching rates is not straightforward owing to a number of sources of variability and uncertainty, including the experimental conditions employed and the nature of the sample considered.

Several aspects of the experimental procedure can significantly influence the rate and magnitude of the HF etching, particularly the temperature of the reaction, its duration, and the concentration of the acid employed (e.g., Leko & Komarova, 1973; Bell & Zimmerman, 1978; Porat et al., 2015). Moreover, earlier studies have shown that, even for a given experimental procedure, etching rate may vary by a factor of > 2 for different quartz samples (Bell & Zimmerman, 1978). In other words, compositionally similar minerals can respond differently to HF treatment, depending on their origin, structure, weathering history or sub-composition. For example, Porat et al. (2015) showed that the mineralogical maturity of a sediment sample has a direct impact on HF etching magnitude.

The most widely used approach to evaluate grain thickness removal during HF etching at a multi-grain level involves weight losses determination: the sample is weighed before and after HF etching in order to estimate the bulk amount of material lost during the etching process (Bell & Zimmerman, 1978, and references therein). Surprisingly, the number of quantitative studies of HF etching rates for quartz and feldspar grains has remained limited since the pioneering works of Fleming (1969) and Bell & Zimmerman (1978). Aside from the assessments of Hong (1998) and, more recently, Porat et al. (2015), little attention has been paid to this question over the last few decades, and the available numerical data in the literature remains scarce or poorly detailed.

In order to provide additional empirical data on this important question, we have performed a series of HF etching experiments on several quartz and feldspar samples of different grain sizes (nominal sieve opening between 50 to 300 µm), using HF at different concentrations (40% and 10%) and durations (10, 20, 40, 60 min). The surface thickness removed by HF etching was calculated through weight loss estimates in order to obtain comparable results with earlier studies.

2. Material

Four commercial natural sand samples were selected for the first two HF etching experiments: three silica sand samples (MS1, MS2 and MS3) and one feldspar-rich sand (MF5). MS1 is a normalized sand (ref. CEN-UNE-EN 196-1) provided by the Instituto de Ciencias de la Construcción Eduardo Torroja (Madrid, Spain) with an initial grain size < 2 mm and a certified SiO_2 content of $> 98\%$. MS-2 is a white sand with an initial grain size of 180-500 µm derived from the Stampian (Oligocene) Fontainebleau sand formation (France). This fined-grain, well-sorted and high purity quartz sand with a SiO_2 content $> 99.5\%$ (French & Worden, 2013) has recently been considered as an appropriate reference material for luminescence dating studies (Kreutzer et al., 2017). MS-3 is a siliceous sand (ref. A-S70) from the Arija Quarry (Spain) and delivered by Sibelco, with a SiO_2 content of $> 90\%$ and an initial grain size of < 1 mm (technical specifications provided by Sibelco). Finally, MF5 is a potassium feldspar sample from Carrascal del Río Quarry (Segovia, Spain), which has been derived from feldspar-rich sands by flotation techniques. Technical specifications provided by Incusa (ref. FK-D) indicate an initial grain size of < 700 µm, a feldspar concentration of $\sim 93\%$ (including $\sim 70\%$ and 23% of K-feldspars and Na feldspars, respectively) and a quartz concentration of $\sim 7\%$.

Another set of 14 natural sediment samples (DY08-9 to DY08-22) was selected for a third HF experiment in order to evaluate the etching rate variability among feldspar grains from a given area. These samples come from alluvial and aeolian deposits preserved on the upper fluvial terrace of the Lena River near Yakutsk in central Siberia (Russia) (Waters et al., 1997).

3. Methods

Sample preparation, HF experiments and Static Image analyses were all carried out at the *Centro Nacional de Investigación sobre la Evolución Humana* (CENIEH, Burgos, Spain).

3.1. HF experiments #1 and #2

Dry sieving was performed on the raw sediment samples (MS1, MS2, MS3 and MF5) using a column of several 200 mm diameter Retsch test sieves of standard mesh sizes ranging from 2 mm to 50 µm. These sieves were mounted on a Retsch AS 200 sieve shaker and sieving time was fixed to 10 min per sample, stopping at intervals of 45 s before restarting. The sediment was collected for standard nominal sieve opening ranges of 100–150 µm and 150–200 µm, which are the most widely used grain sizes in ESR dating of sediment, but also 50–100, 200–250 and 250–300 µm. In order to eliminate possible contamination by other minerals, the sieved fractions were subsequently processed using standard ESR sample preparation techniques: HCl (36%) was used to dissolve carbonates and H_2O_2 (30%) to remove organic matter. Several steps of density separation were carried out using sodium polytungstate (SPT) at d= 2.72, d=2.62 and d=2.58 g/cm^3 (Wintle, 1997) in order to make sure that samples MS-1, MS-2 and MS-3 were only composed of quartz grains and that sample MF-5 only contained potassium feldspars.

Each sample was then divided into several homogenous

Figure 1. Pictures illustrating Experiments #1 (left) and #2 (right).

subsamples (aliquots) by using a Quantachrome Rotary Micro Riffler MRR-11. One aliquot of each sample was kept natural (unetched) and used as a reference, while the others were used for the HF etching experiments. The relative variability in weight among the aliquots of a given sample prior to HF etching was $< 4\%$. Depending on the amount of material available, the initial weight of the subsamples was between 1.5 and 6.5 g.

Two different experiments were performed. For Experiment #1, aliquots of quartz and feldspars (samples MS1, MS2, MS3 and MF5) were transferred to Teflon beakers and covered with 40% or 10% HF for etching times of 10, 20, 40 and 60 min (Figure 1, left). Each beaker was manually agitated and stirred for a few tens of seconds every 5–10 min. For Experiment #2, aliquots of quartz (samples MS1 and MS3) were only treated with 40% HF, and the beakers were placed on a laboratory shaker that agitated the samples along a horizontal plane (Figure 1, right) to ensure more efficient sample mixing and more homogenous etching among grains. An overview of these experimental conditions is provided in Table 1.

HF was systematically added in excess of the selected SiO_2 mass for each sample (between 20 and 60 ml, depending on the aliquot mass considered). Once the required etching duration was reached, the sediment was abundantly rinsed with water (5 times $\sim$200 ml). HCl (30%) was then added in order to remove any remaining soluble fluorides and the sediment was rinsed again, dried overnight at 40 °C and finally weighed. Each set of experiments was carried out within a week at controlled room temperature (25 °C).

3.2. HF experiment #3

14 sediment samples were prepared under subdued red light in the CENIEH Luminescence Dating Laboratory. Coarse-grain K-feldspar fractions were extracted using chemical digestion (30% HCl and H_2O_2 treatment), wet sieving and heavy liquid density separation with 2.53 g/cm^3 and 2.58 g/cm^3 SPT solutions. K-feldspar extracts were transferred to Teflon beakers and etched in 10% HF for 10 minutes following the recommendations of Porat et al. (2015) and treatments adopted in several recent post-IR IRSL K-feldspar dating studies (e.g., Arnold et al., 2014; Demuro et al., 2014). Beakers underwent manual agitation and stirring three times during the etching period (Table 1). The etched K-feldspar fractions were then treated with 30% HCl for 45 minutes to eliminate any acid-soluble fluoride precipitates. The dry weight of each sample was recorded before and after the HF etching procedure, following the same steps outlined in HF experiments #1–2.

To assess the efficiency of our density separation procedures, we measured the bulk K content of two prepared feldspar samples (DY08-21 and DY08-12) using a Risø GM-25-5 beta counter (Bøtter-Jensen & Mejdahl, 1988) at the University of Adelaide's Prescott Environmental Luminescence Laboratory (Australia). For each sample we measured three 100 mg aliquots of prepared material, along with a background standard (MgO) and an aliquot of KCl (known K content = 52.4%; grain size 212–250 μm), following the approach of Bøtter-Jensen & Mejdahl (1985). The bulk K contents of samples DY08-21 and DY08-12 were 12.5 $\pm$ 0.2% and 10.4 $\pm$ 0.2%, respectively, supporting the general purity of the K-feldspar extracts used in Experiment #3.

3.3. Weight loss estimates and associated uncertainty

All of the samples considered in the three experiments were weighed before and after HF etching. A potential source of uncertainty on the weight loss estimates relates to inadvertent grain removal during the washing stages, i.e. when the material is successively rinsed several times with water in order to remove any traces of HF. This potential complication has been assessed in Experiments #1–2 by carrying out an additional control experiment with unetched samples under identical conditions, with the exception that water rather than HF was used during the etching stages. Each blank subsample was washed 10 times to replicate the 5 rinses received following HF treatment and the 5 rinses

Experiment	Samples_Grain size (μm)	HF dilution	Duration of the etching (min)	Comment
#1	MS1_100–150, MS1_150–200, MS2_100–150, MS2_150–200, MS3_100–150, MS3_150–200, MF5_100–150, MF5_150–200	40% and 10%	0, 10, 20, 40 and 60	Manual agitation and stirring every 5–10 min.
#2	MS1_50–100, MS1_100–150, MS1_150–200, MS3_150–200, MS1_200–250, MS1_250–300, MS1_150–200	40%	0, 10, 20, 40 and 60	Continuous agitation
#3	DY08-9 KF_212–250, DY08-10 KF_212–250, DY08-11 KF_212–250, DY08-12 KF_212–250, DY08-13 KF_212–250, DY08-14 KF_212–250, DY08-15 KF_212–250, DY08-16 KF_212–250, DY08-17 KF_212–250, DY08-18 KF_212–250, DY08-19 KF_212–250, DY08-20 KF_212–250, DY08-21 KF_212–250, DY08-22 KF_212–250	10%	10	Manual agitation and stirring undertaken 3 times during the etching period

Table 1. Overview of the three HF etching experiments performed in the present study.

received after HCl treatment in Experiments #1–2. Subsamples were weighed before and after the rinsing process. These control tests were performed with several subsamples of 50–100, 100–150 μm and 150–200 μm fractions of samples MS1, MS2, MS3 and MF-5. As part of Experiment #3, an additional control sample (DY08-7) from the same fluvial terrace site was included to monitor any potential spurious weight losses related to agitation, stirring and rinsing of beakers. Again, this control sample was subjected to exactly the same experimental procedures as the other samples except that water was used instead of 10% HF during the etching stage. The results of these control tests are summarised in Table 2.

Weight losses related to pouring and washing procedures varied within a narrow range (from -2.0 to -3.1%) for 100–200 μm grains in Experiments #1–2 and amounted to -2.7% on average. In contrast, weight losses associated with rinsing were significantly higher for smaller grains, with values ranging from -9.3% for quartz samples to -25.0% on average for feldspar grains. This difference might be due to insufficient waiting times prior to the decantation of the smallest (50–100 μm) grains during the blank experiments. However, despite this uncertainty, one can observe from Figure 2E that all the grain size fractions from 50 to 300 μm have produced consistent weight loss trends (within error) for the main etching tests undertaken in Experiment #2. Consequently, it seems likely that the results obtained from the 50–100 μm fraction during the blank experiment may not be fully representative of the true weight loss uncertainty associated with Experiment #1–2 in this specific case.

In Experiment #3, a relative weight loss of 0% was observed for the larger (212–250 μm) K-feldspar grains of control sample DY08-7 (Table 2). This higher recovery rate compared with Experiment #1-2 may partly be linked to (i) the differences in the sample weights involved in the two sets of blank experiments, i.e. 1.50 g for #3 vs. 0.87–6.37 g for

Experiment	Sample	Grain size (μm)	Initial weight (g)	Final weight (g)	Relative weight loss (%)
#1-2	MF-5	50–100	3.40	2.59	23.8%
#1-2	MF-5	50–100	1.18	0.87	26.3%
#1-2				**Mean**	**25.0%**
#1-2	MS-3	50–100	3.64	3.33	8.5%
#1-2	MS-3	50–100	1.20	1.08	10.0%
				Mean	**9.3%**
#1-2	MS-1	100–150	3.15	3.06	2.9%
#1-2	MS-1	100–150	6.50	6.37	2.0%
#1-2	MS-3	100–150	5.36	5.18	3.4%
				Mean	**2.7%**
#1-2	MS-1	150–200	6.48	6.32	2.5%
#1-2	MS-1	150–200	3.09	3.01	2.6%
#1-2	MS-2	150–200	3.13	3.05	2.6%
#1-2	MS-3	150–200	2.89	2.80	3.1%
				Mean	**2.7%**
#3	DY08-7	212–250	1.50	1.50	0.0%

Table 2. Results of the control tests performed under conditions similar to those of Experiment #1–3, but with water instead of HF, in order to evaluate the minimum weight loss achieved during the washing stage.

#1 and #2, and (ii) the differences in the grain sizes (212–250 μm vs. 50–200 μm).

Together, the control sample results suggest that larger grains are less likely to be affected by weight losses associated with rinsing in our experiments, and that the empirical control data obtained on the larger grain fractions may be considered as more reasonable estimates of the weight loss uncertainties associated with Experiments #1–3.

3.4. Estimates of external surface thickness removal

Grain size analysis of the unetched quartz and K-feldspar samples were performed by static image analyses using a Malvern Instruments Morphologi G3 particle characterization system and Morphologi software 7.41, following the procedure outlined in Duval et al. (2015a). With this technique, 3D particles are captured as high resolution 2D images, from which various size and shape parameters may be derived (e.g., diameter, circularity, elongation, convexity). Among them, the Circle Equivalent (CE) diameter is the diameter of a circle with the same area as the 2D image of the particle. For a given unetched sample, a CE diameter was thus obtained for each particle of the grain population and a mean value and associated error (1 standard deviation) were derived as obtained for each natural sample (see Table 3). The coefficient of variation among the 25 samples overall vary between 8.9% and 14%, except one sample (MS3_100–150 μm) showing a much higher value (48.6%).

Using the mean grain size values and the bulk relative mass loss observed during the three experiments, we calculated the post-etching mean diameter of the grain population of each sample, and estimated the average grain thickness removed by HF etching. The latter is expressed as half of the difference between the pre- and post-HF etching mean diameter. This calculation is based on two major assumptions: (i) the grains have a spherical shape, and (ii) they experienced isotropic and uniform removal of their exterior surfaces during the etching process (Bell & Zimmerman, 1978).

Associated uncertainties on the removed thickness values were derived from a combination of the experimental error on the weight loss estimates (i.e., 3% for 100–200 μm and 9% for 50–100 μm grain size fraction in experiments #1 and #2, and 0% for the K-feldspar samples of experiment #3; see Table 2) and the standard deviation on the mean diameter of a given sample (Table 3).

4. Results

4.1. Weight loss estimates

The following observations can be made from experiments #1, #2 and #3 (numerical values are given in Tables 4, 5, 6 and 7):

Experiment #1

- The feldspar sample (MF5) is more significantly affected by HF (10 or 40%) etching in comparison to the quartz minerals (MS1 to MS3), as would be expected. The 10% HF etching experiments conducted on the 100–150 μm grain size fractions (Table 5) produce a relative weight loss of 24.0% (10 min) to 45.1% (60 min) for MF-5, while the quartz sample weight losses do not exceed 10% (10 min) to 20% (60 min).

Sample	Nominal sieve opening range (μm)	Mineral	Mean CE diameter (μm)	s.d. (μm)	Coefficient of variation (%)
MS1	50-100	Quartz	125.4	17.5	14.0%
MS1	100-150	Quartz	165.3	21.2	12.8%
MS1	150-200	Quartz	207.5	25.0	12.1%
MS1	200-250	Quartz	289.6	31.7	10.9%
MS1	250-300	Quartz	349.8	34.1	9.7%
MS2	100-150	Quartz	177.8	21.1	11.9%
MS2	150-200	Quartz	223.8	25.6	11.4%
MS3	100-150	Quartz	119.3	58.0	48.6%
MS3	150-200	Quartz	220.2	30.4	13.8%
MF5	100-150	K-feldspar	160.9	21.4	13.3%
MF5	150-200	K-feldspar	223.3	26.3	11.8%
DY08-9	212-250	K-feldspar	276.9	28.1	10.1%
DY08-10	212-250	K-feldspar	281.0	28.6	10.2%
DY08-11	212-250	K-feldspar	300.8	28.9	9.6%
DY08-12	212-250	K-feldspar	302.2	31.2	10.3%
DY08-13	212-250	K-feldspar	284.5	25.3	8.9%
DY08-14	212-250	K-feldspar	289.9	26.9	9.3%
DY08-15	212-250	K-feldspar	289.1	27.8	9.6%
DY08-16	212-250	K-feldspar	285.5	26.5	9.3%
DY08-17	212-250	K-feldspar	292.5	28.8	9.9%
DY08-18	212-250	K-feldspar	302.3	30.1	10.0%
DY08-19	212-250	K-feldspar	308.1	29.5	9.6%
DY08-20	212-250	K-feldspar	305.9	30.1	9.8%
DY08-21	212-250	K-feldspar	293.7	29.9	10.2%
DY08-22	212-250	K-feldspar	285.4	35.3	12.4%

Table 3. Mean CE diameter and associated standard deviations (s.d.) and corresponding coefficient of variation obtained by Static Image analysis for each natural (unetched) samples.

In comparison, 100% of the 100–150 μm feldspars are eliminated after 10 minutes of 40% HF etching (Table 4). Similar results are observed for the 150–200 μm feldspars after 40 minutes of 40% HF etching.

- In general, the various quartz samples exhibit similar etching trends, though some are more impacted by HF treatment (MS3) than others (MS2). The 40% HF etching experiments conducted on the 100–150 μm grain size fractions produce relative weight losses of 7.6% (10 min) to 32.5% (60 min) for MS-2, while MS-3 lost between 20.5% (10 min) to 48.4% (60 min) of its initial weight (Table 4).

- As expected, minerals of finer grain size (100–150 μm) exhibited higher relative weight losses compared to coarser grain sizes (150–200 μm). This is explained by the change in surface area to volume ratio that occurs with changes in grain size. For example, 60 min etching with 40% HF caused relative weight losses of 32.5% (MS2) to 48.5% (MS3) for 100–150 μm quartz grains, and 26.0 (MS2) to 40.9% (MS3) for 150–200 μm quartz grains (Table 4).

- A similar HF experiment performed by Hong (1998) (see table 3.1, p.45) on quartz samples with a mean size of 137.5 μm yielded the following weight loss estimates: 38.5 ± 4.2% and 49.1 ± 1.8% for 40% HF etching performed over 40 and 60 min, respectively. These results are systematically higher, but nevertheless consistent within error, with those from Experiment #1: an average weight loss of 31.7 ± 6.6% and 40.7 ± 7.9% was observed in our experiment when undertaking 40% HF etching over 40 and 60 min, respectively, for samples MS1, MS2 and MS3 (100–150 μm fraction).

Experiment #2

- As observed above, an inverse correlation was also observed between grain size and relative weight loss in

Experiment #1 (HF 40%)				
Sample_ Grain Size (μm)	**Time** (min)	**Initial weight** (g)	**Final weight** (g)	**Relative weight loss** (%)
MS-1_100-150	10	6.35	5.54	12.8%
	20	6.55	5.41	17.4%
	40	6.07	4.03	33.6%
	60	6.07	3.57	41.2%
MS-2_100-150	10	2.25	2.08	7.6%
	20	2.26	1.88	16.7%
	40	2.20	1.66	24.4%
	60	2.24	1.51	32.5%
MS-3_100-150	10	5.23	4.16	20.5%
	20	5.22	3.95	24.3%
	40	5.09	3.20	37.1%
	60	5.23	2.70	48.4%
MF-5_100-150	10	3.38	0.05	98.4%
	20	3.48	0.10	97.1%
	40	3.47	0	100.0%
	60	3.32	0	100.0%
MS-1_150-200	10	6.21	5.54	10.8%
	20	6.41	5.52	13.9%
	40	6.48	5.08	21.6%
	60	6.54	4.35	33.5%
MS-2_150-200	10	6.42	6.02	6.2%
	20	6.46	5.85	9.4%
	40	6.23	5.09	18.3%
	60	6.28	4.65	26.0%
MS-3_150-200	10	2.80	2.34	16.5%
	20	2.84	2.16	24.1%
	40	2.84	1.77	37.6%
	60	2.79	1.65	40.9%
MF-5_150-200	10	4.02	1.05	73.9%
	20	4.10	1.30	68.2%
	40	4.33	0.05	98.8%
	60	4.17	0.03	99.3%

Table 4. Weight loss data derived from Experiment #1 (HF 40%).

Experiment #1 (HF 10%)				
Sample_ Grain Size (μm)	**Time** (min)	**Initial weight** (g)	**Final weight** (g)	**Relative weight loss** (%)
MS-1_100–150	10	3.35	3.18	5.1%
	20	3.22	3.04	5.6%
	40	3.29	3.02	8.2%
	60	3.31	3.01	9.1%
MS-2_100–150	10	1.57	1.55	1.3%
	20	1.57	1.53	2.2%
	40	1.57	1.52	3.2%
	60	1.57	1.51	4.0%
MS-3_100–150	10	2.67	2.48	7.1%
	20	2.69	2.46	8.6%
	40	2.61	2.31	11.5%
	60	2.73	2.34	14.3%
MF-5_100–150	10	2.77	2.10	24.0%
	20	2.84	2.06	27.6%
	40	2.80	1.78	36.3%
	60	2.98	1.63	45.1%
MS-1_150–200	10	3.26	3.23	0.9%
	20	3.32	3.25	2.1%
	40	3.20	3.11	2.8%
	60	3.24	3.06	5.6%
MS-2_150–200	10	3.08	3.06	0.6%
	20	3.02	3.00	0.7%
	40	3.20	3.12	2.5%
	60	3.21	3.12	2.8%
MS-3_150–200	10	2.83	2.68	5.4%
	20	2.81	2.59	8.0%
	40	2.82	2.63	6.8%
	60	2.85	2.54	10.8%
MF-5_150–200	10	3.57	3.03	15.0%
	20	3.84	3.16	17.7%
	40	3.80	2.78	26.8%
	60	3.69	2.57	30.4%

Table 5. Weight loss data derived from Experiment #1 (HF 10%).

Experiment #2, with higher grain sizes displaying lower relative weight losses (Table 6). For instance, to achieve a 25% relative weight loss for 50–100 μm, 150–200 μm and >200 μm quartz grain sizes, it was necessary to undertake 40% etching for 10 min, 25 min and 40 min, respectively.

- As with Experiment #1, the results of Experiment #2 show that there may be some differences in weight loss depending on the quartz sample under consideration. In this case, sample MS3 is consistently affected by HF etching to a greater extent than sample MS1 (Table 6).
- Three samples were used in both Experiments #1 and #2 (MS1_100–150 μm, MS1_150–200 μm and MS3_150–200 μm). The comparisons of these results (Table 4 and 6) show that, for a given sample, the weight loss after 10 mins of etching is virtually the same in each experiment, but the difference in weight loss significantly increases with time. Relative weight loss systematically exceeded 50% for these samples in Experiment #2, whereas it did not exceed 50% for the corresponding samples tested in Experiment #1. Such a difference could be intuitively expected, although it has never been

Experiment #2 (HF 40%) – with constant agitation				
Sample_ Grain Size (μm)	**Time** (min)	**Initial weight** (g)	**Final weight** (g)	**Relative weight loss** (%)
MS-1_50–100	10	0.84	0.65	23.2%
	20	0.98	0.64	34.0%
	40	0.94	0.41	56.4%
	60	1.04	0.29	72.2%
MS-1_100–150	10	3.31	2.84	14.3%
	20	3.21	2.37	26.0%
	40	3.31	1.65	50.1%
	60	3.15	0.93	70.4%
MS-1_200–250	10	2.63	2.47	6.1%
	20	2.69	2.38	11.6%
	40	2.70	2.00	26.1%
	60	2.68	1.52	43.2%
MS-1_150–200	10	3.16	2.82	10.7%
	20	3.28	2.63	19.7%
	40	3.18	1.87	41.2%
	60	3.00	1.25	58.3%
MS3_150–200	10	2.78	2.28	18.0%
	20	2.73	1.90	30.3%
	40	2.75	1.21	56.2%
	60	2.86	0.69	75.8%
MS1_250–300	10	3.05	2.90	5.1%
	20	3.01	2.70	10.3%
	40	3.12	2.37	24.0%
	60	3.08	1.83	40.5%

Table 6. Weight loss data derived from Experiment #2 (HF 40%) with constant agitation.

properly quantified. A couple of causes may be envisaged. During HF experiment #1, the grains formed a layer of a few mm thick in the beaker. Consequently, without agitation there may be significant differences in terms of etching rates between the grains that are located on top of the layer and those positioned within the layer. Grains in the latter category might simply not be fully in contact with the chemical reagent given their compaction. The constant agitation undertaken during Experiment #2 ensures that the total surface area of the grains is in direct contact with the chemical reagent during the entire reaction. In other words, a greater proportion of grains are exposed to more uniform etching conditions during agitation, resulting in higher weight loss estimates. Another explanation could be the local neutralization or depletion of HF in the immediate surrounding of the grains if no agitation occurs, which may slow down or partly buffer the etching effects over the entire duration of the experiment.

Experiment #3 (HF 10%) – 3 × manual agitation and stirring during the etching period				
Sample	**Time** (min)	**Initial weight** (g)	**Final weight** (g)	**Relative weight loss** (%)
DY08-9	10	1.13	0.88	22.1%
DY08-10	10	1.27	0.98	22.8%
DY08-11	10	1.23	0.93	24.4%
DY08-12	10	1.20	0.92	23.3%
DY08-13	10	1.09	0.83	23.9%
DY08-14	10	0.80	0.53	33.7%
DY08-15	10	0.52	0.40	23.1%
DY08-16	10	0.58	0.42	27.6%
DY08-17	10	0.68	0.52	23.5%
DY08-18	10	1.21	0.94	22.3%
DY08-19	10	1.01	0.78	22.8%
DY08-20	10	0.89	0.70	21.3%
DY08-21	10	1.01	0.77	23.8%
DY08-22	10	1.08	0.83	23.1%

Table 7. Weight loss data derived from Experiment #3 (HF 10% during 10 min).

Experiment #3

- On average, the net dry weight of the fourteen K-feldspar samples was reduced by 24.3% after 10% HF etching for 10 minutes. The weight loss values observed for individual samples is fairly consistent, ranging between 20–25% for all but two of the fourteen samples (Table 7). The remaining two samples display slightly higher weight losses of up to 34%, highlighting that inter-sample variability exists for this geographic location. The weight losses observed for the fourteen K-feldspar samples in Experiment #3 are broadly similar to those observed for K-feldspar sample MF5 in Experiment #1, which was conducted under similar experimental conditions (MF5 weight losses = 24% for 100–150 μm grains and 15% for 150–200 μm grains).

4.2. Removed thickness estimates

The weight loss results have been converted into estimates of removed thickness as indicated in section 3.4. Results are graphically displayed in Figures 2 (Experiments #1 and #2) and 3 (Experiment #3). The corresponding numerical values are given in the Supplementary Information (Table S1 to S4).

4.2.1 Identifying external factors influencing etching rates

As would be expected, the grain thickness removed by HF etching increases almost linearly with time. When us-

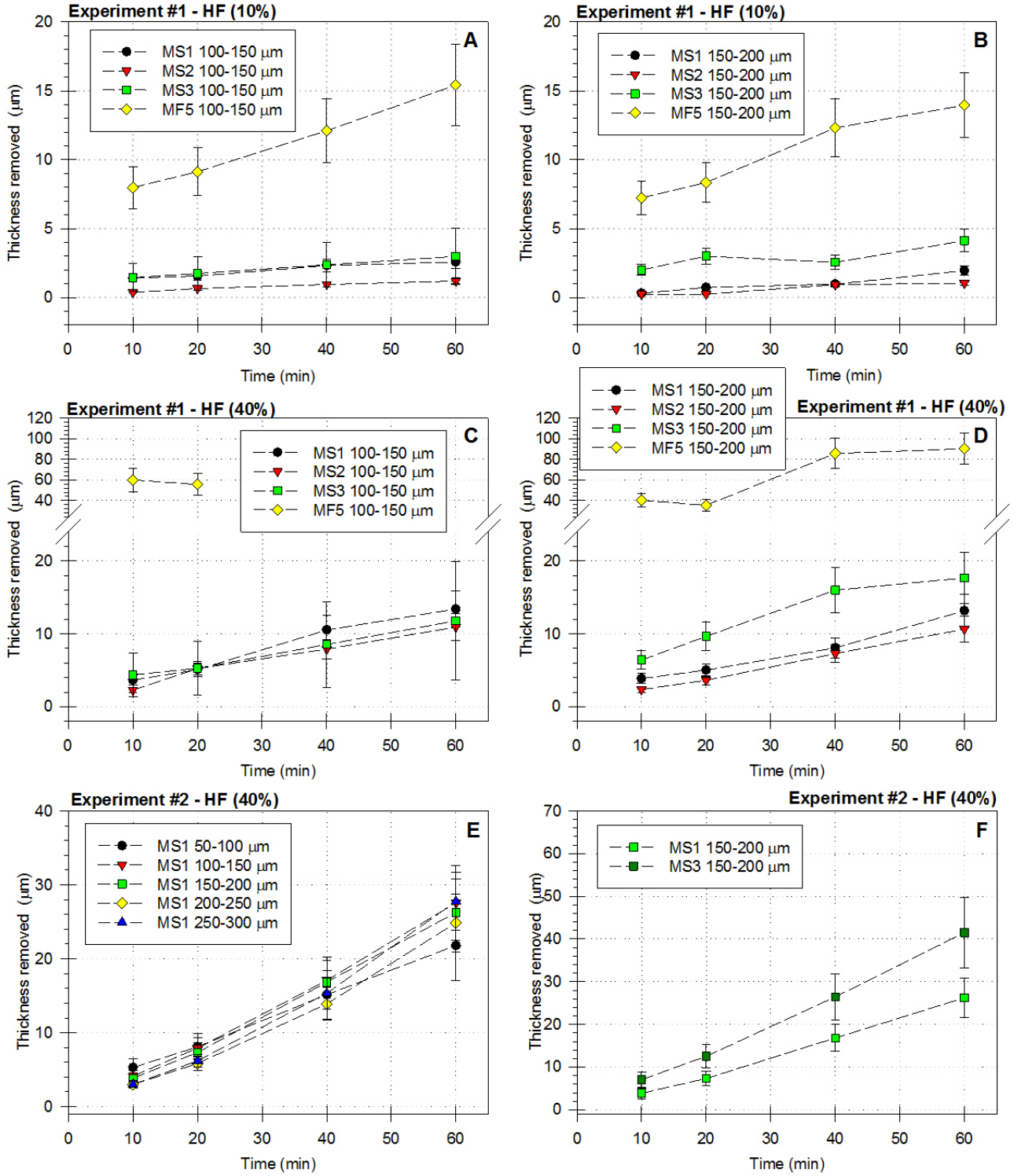

Figure 2. Relationship between grain thicknesses removed from quartz and feldspar samples and HF (10% and 40%) etching duration for Experiments #1 (A to D) and #2 (E and F).

ing 40% HF, the average etching thicknesses ranged from 3.8 ± 1.5 µm after 10 min to 12.9 ± 2.6 µm after 1 hr for 100–200 µm quartz samples (Fig. 2C, Table 8). In contrast, a significantly smaller dependency is observed between etching thickness and time when using 10% HF; grain thickness removal increases by only a factor of ∼2.3 over 10 min to 1 hr etching times (Fig. 2A). After 60 min, 10% HF has only removed a mean external thickness of 2.3 ± 1.2 µm from the quartz grains.

As expected, 40% HF has a more significant impact on

Mineral	Quartz	Quartz	Quartz	K-feldspar	K-feldspar	K-feldspar
Experiment	#1	#2	#1	#1	#1	#3
HF concentration	40% HF	40% HF	10% HF	40% HF	10% HF	10% HF
Sample size	n=6	n=6	n=6	n=2	n=2	n=14
Time (min)						
10	3.8 ± 1.5 µm (39.6%)	4.4 ± 1.5 µm (35.3%)	1.0 ± 0.8 µm (77.3%)	50.2 ± 14.0 µm (28.0%)	7.6 ± 0.5 µm (6.9%)	12.9+1.8m (14.3%)
20	5.7 ± 2.1 µm (36.2%)	8.0 ± 2.4 µm (30.0%)	1.3 ± 1.0 µm (75.3%)	45.5 ± 14.3 µm (31.4%)	8.7 ± 0.5 µm (6.3%)	-
40	9.7 ± 3.3 µm (33.6%)	17.5 ± 4.6 µm (26.2%)	1.7 ± 0.8 µm (47.6%)	85.8 ± 14.5 µm (16.9%)	12.2 ± 0.1 µm (1.2%)	-
60	12.9 ± 2.6 µm (19.9%)	28.3 ± 6.8 µm (24.2%)	2.3 ± 1.2 µm (50.2%)	90.4 ± 15.3 µm (16.9%)	14.7 ± 1.0 µm (7.0%)	-

Table 8. Average removed thicknesses and associated standard deviation (in parenthesis, the corresponding coefficient of variation) evaluated from the weight loss estimates of all samples and grain size fractions considered in each experiment (#1, #2 and #3). To obtain the post-etching grain diameter, the thickness values should be multiplied by two and then subtracted from the initial grain diameters displayed in Table 3. Key: n = number of samples considered for the mean value.

quartz grains than 10% HF, removing external layers that are 4–6 times thicker over 10 and 60 min etching periods (Fig. 2A to D). The results of Experiment #2 confirm that constant agitation of samples has a direct influence on etching rates when using 40% HF. For example, sample MS1 experienced mean grain thickness losses of 3.7 to 13.4 µm for 10 and 60 min etching durations in Experiment #1 (no agitation), whereas equivalent losses of 4.1 to 27.6 µm were observed over the same etching time ranges in Experiment #2 (constant agitation) (Fig. 2C and E). The differences between the results of Experiments #1 and #2 increase significantly over longer etching times; mean grain thickness removals are 12% higher in Experiment #2 compared to Experiment #1 after 10 min, and they are 106% higher in Experiment #2 compared to Experiment #1 after 60 min.

In summary, these empirical results show that experimental conditions have a significant impact on etching rate and magnitude. Though the influence of etching time and HF concentration has already been demonstrated in several previous studies, the role of agitation has, to our knowledge, not been explicitly reported or thoroughly evaluated so far.

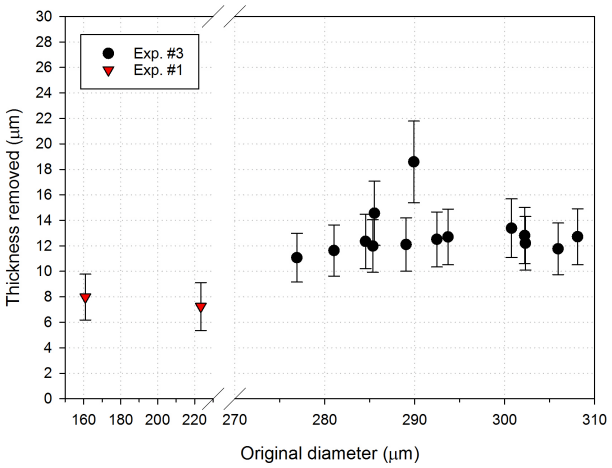

Figure 3. Variability of grain thickness removal from K-feldspar samples derived from Experiment #3. For comparison, data obtained from sample MF-5 during experiment #1 under somewhat similar conditions (HF 10%) are also displayed.

4.2.2 Variability among quartz and K-feldspar samples

Variability in etching effects among different quartz samples is best illustrated by Fig. 2D. For the 150–200 µm quartz samples considered in Experiment #1, MS3 experiences more significant etching losses compared to MS1 and MS2 over 10–60 min etching times. The latter two samples exhibit broadly similar etching thicknesses (within error) over the same time periods. For all three samples, thickness removals range from 2.4 to 6.4 µm after a 10 min etching duration, to 10.7–17.7 µm after 60 min of etching. The same variability in etching magnitude between samples MS-1 and MS-3 is observed in Experiment #2 (Fig. 2F).

In contrast with our previous observations on weight loss estimates, initial grain size appears to have no significant impact on mean removed thicknesses: Experiment #2, which was performed on 50–300 µm (nominal sieve size) grains of sample MS1, reveals consistent mean thicknesses (within error) for all grains size fractions after a given etching time (Fig. 2E). Similarly, 100–150 µm and 150–200 µm K-feldspar fractions of samples MF5 show similar etching thicknesses when using 10% HF for different durations (Fig. 2A and B).

Given these observations, we have calculated average etching thickness values and associated standard deviations

for a given experiment based on a combination of all the samples and grain fractions analysed in each of Experiments #1, 2 and 3 (Table 8). The coefficients of variation for the quartz samples (n=6) analysed during Experiments #1 and #2 range from ∼20% to ∼77% (the reliability of the equivalent values obtained for the K-feldspars are considered relatively uninformative given the limited number of samples considered, n=2). Interestingly, one may observe that very high coefficients of variation are seen when etching is limited (10–20 min). All samples show a common pattern of a decreasing variability with time, with overall minimum values achieved in the range of 20–35% for 40 and 60 minutes. This may be explained by the increasing elimination of the finer grain population with time, resulting in a narrower grain size distribution.

Overall, these coefficient of variation data provide useful insights into inter-sample variability of etching rates, which incorporates both experimental uncertainty (from the washing and weighing stages; though the latter is likely minimal) and inherent variability related to mineralogical maturity, composition, geological origin and grain-to-grain heterogeneities. Based on the present results, the intrinsic relative uncertainty on removed thickness for etched quartz grains is likely to be at least 20% after 40–60 min for a given set of experimental conditions, and can be as high as ∼35% (Table 8).

The variability in etching thicknesses between K-feldspar samples is best observed from Experiment #3 (Fig. 3). The 14 samples considered in this experiment exhibit a mean reduction in grain thickness of 12.9 ± 1.8 µm after etching with 10% HF for 10 min (Table 8). The combined dataset has a coefficient of variation of 14.3%, which is lower than that measured for the quartz samples in Experiments #1–2 (between ∼20% and ∼77%). Given that all 14 K-feldspar samples were collected from a single site, this dataset may provide useful first order constraint on etching rate variability for samples of shared geographic origin. Some variability exists between the etching thicknesses observed in Experiments #1 and #3 for different K-feldspar samples. The K-feldspar removal thicknesses derived from Experiment #1 are smaller (7.6 ± 0.5 µm on average) than those obtained in Experiment #3 (Fig. 3 and Table 8). This difference may reflect differences in the experimental conditions (e.g., different initial sample weights, different agitation and stirring procedures employed in the two experiments), inter-sample variability in K-feldspar etching rates, or, most likely, a combination of both factors.

5. Discussion

5.1. Comparison with previously published results

The majority of luminescence and ESR quartz dating procedures utilise concentrated (40–48%) HF etching for either 40 min or 60 min durations. These various combinations are adopted on the assumption that they would be sufficient to remove a ∼10 µm thick layer from the exterior surface of quartz grains, in accordance with the results from Bell & Zimmerman (1978) and Fleming (1969), respectively. In reality, the weight loss experiments carried out by Bell & Zimmerman (1978) on two different quartz samples revealed more complex results: while one quartz sample that was immersed in 40% HF for 40 min showed an average depth loss of ∼10 µm, the other sample was significantly less affected by the same etching procedure (∼3 µm). These results underscore the inter-sample variability observed in our own experiments. Aitken (1985) mentions the results of a similar HF etching experiment performed on quartz samples by Fleming (1969), for which a ∼9 µm removal was observed after 60 min of 40% HF exposure. This result is likely compatible with the ∼10 µm loss recorded after 40 min by Bell & Zimmerman (1978), as the associated empirical uncertainty of these two experiments was not reported. By comparison, the etched thicknesses obtained in the present study from Experiment #1 (40 min and 60 min exposure to 40% HF) are 9.7 ± 3.3 µm and 12.9 ± 2.6 µm, respectively (Table 8). These results are consistent with the published estimates mentioned above, as well as with those reported by Hong (1998) (i.e., 10.3 ± 1.9 µm and 13.8 ± 1.4 µm for 40 and 60 min of 40% HF, respectively). However, it is worth keeping in mind that mean removed thicknesses were almost twice as high over the same time range when the samples were continuously agitated during HF etching (Experiment #2; see Table 8).

In contrast with quartz dating procedures, there appears to be less standardisation in HF etching procedures adopted in K-feldspar luminescence studies, although there is an apparent overall consensus to avoid the use of concentrated HF (> 40%), even for short durations. Some luminescence practitioners prefer not to include a HF etching step during sample preparation (Duller, 1992; Trauerstein et al., 2014), while others use various combinations of dilute (10%) HF over relatively short etching durations (typically 10 min to 40 min) to remove the outer alpha-irradiated layers of coarse grains (Mejdahl, 1985; Li & Li, 2011; Demuro et al., 2015). The reasons behind these choices of experimental conditions, and especially the different durations, are not always stated (but see Duller, 1992, section 3.2.2.), and they are most likely based on individual laboratory recipes and unpublished studies. Indeed, quantitative assessments of K-feldspar etching rates are scarce in the literature. Porat et al. (2015) reported a decrease in the modal size of 50 and 100 µm K-feldspar grains after 20 and 40 min of exposure to 10% HF, respectively. Consequently, they considered that 10% HF etching for 10-15 minutes should be sufficient to remove most of the outer surface affected by alpha particles. In contrast, longer durations would favour further etching anisotropy for a given grain (see also Duller, 1992) and etching heterogeneity among grains, resulting thus in additional complications and increased uncertainty for dose rate evaluation. We have observed an average K-feldspar depth loss of 12.9 ± 1.8 µm after 10 min etching with 10% HF for 14 samples in Experiment #3 (Table 8), which is consistent with the observations of Porat et al. (2015). However, Experiment #1 also

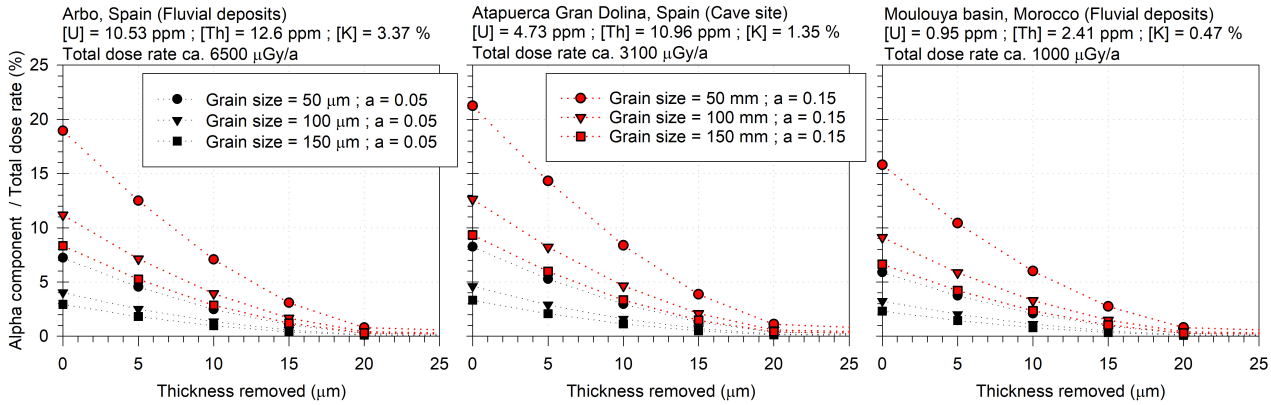

Figure 4. Relationship between relative alpha dose rate contributions (relative to the total dose rate) and assumed HF etching depths for quartz of initial grain size of 50, 100 and 150 µm and an alpha efficiency of 0.05 and 0.15. Three existing case studies are displayed from left to right (in decreasing order with respect to the magnitude of the total dose rate): Arbo (Spain), Atapuerca Gran Dolina (Spain) and Moulouya basin (Morocco). Calculations were performed using the following parameters: internal dose rate = 30 µGy/a, cosmic dose rate = 110 µGy/a, water content = 10% wet weight (equivalent to 11% dry weight), and water correction factors, alpha and beta attenuations, and etching depth corrections from the DRAC data compilation spreadsheet (Supplementary material from Durcan et al. (2015)).

showed lower K-feldspar etching depths of 7.6 ± 0.5 µm for an additional sample. Taken together, 10% HF for 10 min seems to be sufficient to remove the targeted alpha-affected outer ~ 10 µm rind of most coarse K-feldspar grain fractions considered so far; though additional empirical data is needed to better characterise inter-sample variability in K-feldspar etching efficiencies.

5.1.1 Minimum recommended HF etching depth

Although the maximum penetration range of alpha particles in silicate grains is usually considered to be ~ 20 µm, the attenuation factors provided by Bell (1979) show that such an etching depth would not entirely remove the external alpha dose rate component ($\sim 96\%$ would be eliminated). Etching depths of 15, 10 and 5 µm would remove ~ 85, ~ 66 and ~ 38 % of the external alpha dose rate component, respectively. Consequently, it is worth considering whether the 10 µm etching depth usually targeted in ESR and luminescence dating is sufficient to reduce the alpha dose rate contribution to negligible levels in comparison with the total dose rate. Simulations performed by Bell (1979) suggest that a 9 µm etching depth would reduce the external alpha dose rate component to between 2 and 10% of the total dose rate, depending on the alpha efficiency selected (0.05–0.1) and the relative concentration of potassium in the sediment (0 to 2% K_20). For comparison, we ran a series of simulations with three quartz samples collected from different localities (Arbo and Atapuerca Gran Dolina, Spain and the Moulouya basin, Morocco) that contain low to high radioactivity deposits (1,000 to 6,500 µGy/a). In each simulation we considered different grain sizes (50 to 150 µm) and alpha efficiency values that encompass those commonly used in luminescence and ESR dating, (0.05 and 0.15, respectively; e.g. Arnold et al. (2014); Duval et al. (2015b)) (Fig. 4). Our results show that, in all but one extreme scenario (50 µm grain size and alpha efficiency = 0.15), a 5 µm etching depth is sufficient to reduce alpha dose rate contributions to $<10\%$ of the total dose rate. The alpha dose rate contributions are further reduced to $<5\%$ and $<2.5\%$ of the total dose rate for 10 µm and 15 µm etching depths, respectively. Though relatively small, these alpha dose rate contributions may be non-negligible, and it may be worth considering an additional alpha dose rate term as part of the ESR and luminescence age calculation when etching depths are <15 µm.

Although use of increasing HF etching times may be considered as an alternative means of reaching a depth removal >15 µm and thus completely eliminating alpha dose rate contributions, this approach is likely to raise additional problems, as outlined by Bell & Zimmerman (1978). In particular, more stringent HF procedures are likely to increase inter-grain etching heterogeneity and they cannot guarantee that external alpha contributions will truly be removed from all grains. Consequently, Aitken (1985) and Bell & Zimmerman (1978) consider HF removal of the outer 10 µm of silicate grains to represent the most reasonable compromise for dose rate evaluation.

6. Conclusion

Quantification of HF etching effects is essential for the evaluation of the alpha and, to a lesser extent, beta dose rate components in ESR and luminescence dating. Etching thicknesses ranging from 0 to 20 µm have relatively limited impact on the resulting beta dose rate of quartz grains ($<2\%$), whereas the alpha dose rate may be reduced by up to 96% (see Aitken, 1985). Building on the earlier work of Fleming (1969) and Bell & Zimmerman (1978), which still stand as references in luminescence and ESR dating, our study provides additional, detailed empirical data highlighting the variability of etching rates as a function of experimental conditions and sample type. Based on our results, the outer

10 µm rind of quartz samples (i.e., the usual target in ESR and luminescence dating studies) can be removed by etching with 40% HF for 40 min when including periodic manual agitation, or by etching with 40% HF for $\sim$20 min when undertaking continuous agitation. For K-feldspars, etching with 10% HF for between 10 and 40 min was required to remove the outer 10 µm rind of the samples considered in this study. These results are in good agreement with previous etching assessment studies, although we recommend that each laboratory evaluates etching thickness losses (and associated empirical uncertainties) for their specific HF experimental setup given the observed variability of etching rates. HF etching depths of between 5 and 15 µm will significantly reduce external alpha dose rate contributions to <2.5 – <10% of the total dose rate (depending on the alpha efficiency value used). Although relatively small, this contribution is nevertheless non-negligible. Consequently, it may be worthwhile to consider an additional alpha dose rate term as part of the ESR and luminescence age calculation when etching depths are <15 µm.

Finally, the reliability of HF etching depths based on weight loss estimates is directly dependent on the validity of two important assumptions, i.e. the spherical shape of the grains, and isotropic HF etching of individual grains, as well as collective grain populations, for a given sample. Although these assumptions are known to be oversimplistic (e.g., Bell & Zimmerman, 1978; Goedicke, 1984; Duval et al., 2015a), their true impact on the accuracy of empirical etching depth calculations remains unstudied and largely unconstrained. Preferential dissolution has been observed along crystallographic directions (e.g., Tellier & Jouffroy, 1983), fissures and grain boundaries (Porat et al., 2015), systematically inducing uneven etching at both single-grain and multi-grain scales (e.g., Duller, 1992), which may sometimes result in grain disintegration. The magnitude of HF etching among different grains of a given sample may significantly vary, with potentially non-trivial implications for single-grain OSL dating studies. In that regard, comparative assessments of standard weight loss assessments with different quantitative approaches such as Static Image Analysis (Duval et al., 2015a) and Laser Diffraction should enable further insights into the impact of uneven HF etching at both single and multi-grain levels.

Acknowledgments

This study received funding from Australian Research Council Future Fellowship FT150100215 and FT130100195. MD would like to thank M. Bartz (University of Cologne, Germany) for sharing the data of a sediment sample from the Moulouya basin (Morocco). Finally, the constructive comments by G.A.T. Duller and an anonymous reviewer on an earlier version of the manuscript have contributed to improve the quality of this work.

References

Aitken, M.J. *Thermoluminescence Dating*. Academic Press, London, 1985.

Arnold, L.J., Demuro, M., Parés, J M., Arsuaga, J.L., Aranburu, A., Bermúdez de Castro, J.M., and Carbonell, E. *Luminescence dating and palaeomagnetic age constraint on hominins from Sima de los Huesos, Atapuerca, Spain.* Journal of Human Evolution, 67: 85–107, 2014.

Bell, W.T. *Attenuation factors for the absorbed radiation dose in quartz inclusions for thermoluminescence dating*. Ancient TL, 8: 2–13, 1979.

Bell, W.T. and Zimmerman, D.W. *The Effect Of HF Acid Etching On The Morphology Of Quartz Inclusions For Thermoluminescence Dating*. Archaeometry, 20(1): 63–65, 1978.

Bøtter-Jensen, L. and Mejdahl, M. *Determination of potassium in feldspars by beta counting using a GM multicounter system*. Nuclear Tracks and Radiation Measurements, 10: 663–666, 1985.

Bøtter-Jensen, L. and Mejdahl, M. *Assessment of beta dose-rate using a GM multicounter system*. Nuclear Tracks and Radiation Measurements, 14: 187–191, 1988.

Demuro, M., Arnold, L.J., Parés, J M., Pérez-González, A., Ortega, A.I., Arsuaga, J.L., Bermúdez de Castro, J.M., and Carbonell, E. *New luminescence ages for the Galería Complex archaeological site: Resolving chronological uncertainties on the Acheulean record of the Sierra de Atapuerca, northern Spain*. PLOS ONE, 9: e110169, 2014.

Demuro, M., Arnold, L.J., Parés, J M., and Sala, R. *Extended-range luminescence chronologies suggest potentially complex bone accumulation histories at the Early-to-Middle Pleistocene palaeontological site of Huéscar-1 (Guadix-Baza basin, Spain)*. Quaternary International, 389: 191–212, 2015.

Duller, G.A.T. *Luminescence Chronology of Raised Marine Terraces, South-West North Island, New Zealand*. PhD thesis, Institute of Earth Studies, University of Wales, Aberystwyth, 1992.

Durcan, J.A., King, G.E., and Duller, G.A.T. *DRAC: Dose rate and age calculator for trapped charge dating*. Quaternary Geochronology, 28: 54–61, 2015.

Duval, M., Campaña, I., Guilarte, V., Miguens, L., Iglesias, J., and González Sierra, S. *Assessing the uncertainty on particle size and shape: Implications for ESR and OSL dating of quartz and feldspar grains*. Radiation Measurements, 81: 116–122, 2015a.

Duval, M., Sancho, C., Calle, M., Guilarte, V., and Peña-Monné, J.L. *On the interest of using the multiple center approach in ESR dating of optically bleached quartz grains: Some examples from the Early Pleistocene terraces of the Alcanadre River (Ebro basin, Spain)*. Quaternary Geochronology, 29: 58–69, 2015b.

Fleming, S.J. *The acquisition of radioluminescence by ancient ceramics*. Unpublished D. Phil Thesis, Oxford University, 1969.

French, M.W. and Worden, R.H. *Orientation of microcrystalline quartz in the Fontainebleau Formation, Paris Basin and why it preserves porosity*. Sedimentary Geology, 284–285(0): 149–158, 2013.

Goedicke, C. *Microscopic investigations of the quartz etching technique for TL dating.* Nuclear Tracks and Radiation Measurements (1982), 9(2): 87–93, 1984.

Hong, D.-G. *Luminescence stimulated from quartz by green light developments relevant to dating*. Unpublished D. Phil Thesis, University of Edinburgh, 1998.

Kreutzer, Sebastian, Friedrich, Johannes, Sanderson, David, Adamiec, Grzegorz, Chruścińska, Alicja, Fasoli, Mauro, Martini, Marco, Polymeris, George S., Burbidge, Christopher I., and Schmidt, Christoph. *Les sables de Fontainebleau: A Natural Quartz Reference Sample and its Characterisation*. Ancient TL, 35(2): 21–31, 2017.

Leko, V K. and Komarova, L.A. *Kinetics of the etching of quartz glass in hydrofluoric acid.* State Scientific-Research Institute of Quartz Glass. Translated from Steklo i Keramika 11: 15, 1973.

Li, B. and Li, S.-H. *Luminescence dating of K-feldspar from sediments: A protocol without anomalous fading correction*. Quaternary Geochronology, 6(5): 468–479, 2011.

Mejdahl, V. *Thermoluminescence dating based on feldspars*. Nuclear Tracks and Radiation Measurements (1982), 10(1): 133–136, 1985.

Porat, N., Faerstein, G., Medialdea, A., and Murray, A.S. *Re-examination of common extraction and purification methods of quartz and feldspar for luminescence dating*. Ancient TL, 33(1): 22–30, 2015.

Tellier, C.R. and Jouffroy, F. *Orientation effects in chemical etching of quartz plates*. Journal of Materials Science, 18: 3621–3632, 1983.

Trauerstein, M., Lowick, S.E., Preusser, F., and Schlunegger, F. *Small aliquot and single grain IRSL and post-IR IRSL dating of fluvial and alluvial sediments from the Pativilca valley, Peru*. Quaternary Geochronology, 22: 163–174, 2014.

Waters, M. R., Forman, S. L., and Pierson, J. M. *Diring Yuriakh: A Lower Paleolithic Site in Central Siberia*. Science, 275(5304): 1281–1284, 1997.

Wintle, A.G. *Luminescence dating: Laboratory procedures and protocols*. Radiation Measurements, 27: 769–817, 1997.

Reviewer

Geoff Duller

Thesis Abstracts

Index

Janina J. Bösken p. 15
Yan Li p. 16
Stefania Cristino de Oliveira p. 16
Marius Pfeifer p. 17

Janina J. Bösken

Luminescence dating of eolian and fluvial archives in the Middle and Lower Danube catchment and the paleoenvironmental implications

February 2018

Geographical Institute, RWTH Aachen University, Germany

Degree: Dr. rer. nat.
Supervisors: Frank Lehmkuhl, Helmut Brückner

The presented doctoral dissertation uses luminescence dating techniques to reconstruct the paleoenvironmental and paleoclimatic conditions in the Middle and Lower Danube catchments, especially during the period of anatomically modern human emergence. It is embedded in the Collaborative Research Centre 806 "Our Way to Europe - Culture-Environment Interaction and Human Mobility in the Late Quaternary". To increase ones understanding of the environmental conditions during the last 150 ka, four loess-paleosol sequences (LPS) and one fluvial section were investigated. The research area is located at the junction of Atlantic, Mediterranean and continental climatic regimes, which makes it sensitive to climatic changes. Moreover, the geographical position between Asia, Near East and Central Europe and the vast river network connecting these regions, make the area a favorable pathway for anatomically modern human migration. The sediments of the five investigated sites cover various time-frames from the penultimate interglacial to the Holocene. The methodological approach focused on optically stimulated luminescence dating, but for some of the sections the geochronological methods were combined with physical, biological, and geochemical proxy data to reconstruct the paleoenvironmental conditions.

In the Middle Danube Basin (MDB) three sites were investigated. The Ságvár LPS is located in the central basin and its sediments accumulated during the last glacial maximum from approximately 25–17ka. The sequence can be correlated to two Gravettian occupation layers. Paleoenvironmental conditions changed rapidly and Gravettian occupation took place during a typically cold LGM phase. The Bodrogkeresztúr LPS is located in the foothills of the Carpathians in the northern part of the MDB. Its sediments accumulated between 33.5 $\pm$ 2.5 and 28.0 $\pm$ 2.1 ka and the findings highlight unique microclimatic conditions at the foothills of the Carpathian Mountains, which may have offered a favorable environment for Upper Paleolithic populations. The Crvenka-At site contains fluvial sediments and Aurignacian artifacts that were found in sediments with an age between 33.9 $\pm$ 2.9 ka and 41.3 $\pm$ 3.6 ka. This age range fits well to other dated Aurignacian findings in the Banat region and points to a more widespread occurrence of anatomically modern humans during this time frame than previously thought and shows that also lowland areas were attractive for early modern human occupation. Further south, the Stalać section is located in the interior of the Central Balkan region, in a zone of paleoclimatic shifts between continental and Mediterranean climate regimes. Detailed investigations on the luminescence signal of a quartz sample, which is unsuitable for dating, are presented. A firm chronology framing the last two glacial cycles was established using fine-grained polyminerals and the post-infrared infrared stimulated luminescence (pIRIR) protocol. The characteristics of the dated paleosols indicate similar climatic conditions during the last interstadial and interglacial phases, which were different from the penultimate interglacial period. Finally, the Urluia LPS in the Lower Danube Basin was investigated. The section was dated from 20.98 $\pm$ 1.6 ka to 144.9 $\pm$ 12.2 ka. While the chronology of the upper 7 m of the section is supported by independent age control in form of the Campanian Ignimbrite/Y-5 tephra, the lower part of the sequence remains less well constrained. A rapid increase in ages between $\sim$7 and 9 m is followed by rather constant ages $>$130ka in the lower 7 m of the profile. These ages are in contrast with the expectation of a well-developed MIS5 paleosol in the lowermost part of the section. Several hypothesis trying to explain these findings were explored, but could not be solved satisfactorily.

The doctoral dissertation demonstrates that a detailed investigation is necessary in order to build robust age models. For quartz samples, the importance of preheat plateau and dose recovery tests are pointed out. Some samples of Stalać and Urluia, that have high equivalent doses, show falling preheat plateaus, while the quartz samples of Crvenka-At are already in saturation at very low doses. These findings indicate that these samples cannot be dated reliably using the SAR protocol. Most samples of this dissertation were dated with the pIRIR protocol. The necessary first IR stimulation temperature tests, dose recovery tests, fading experiments and residual dose measurements are presented. It is demonstrated that polymineral and potassium feldspar samples can be dated with higher doses than quartz. However, it remains unclear up to which dose range age estimates are

reliable. Overall, this doctoral dissertation highlights the importance of luminescence dating in paleoenvironmental and geoarcheological studies. It demonstrates how the combination of multiple proxy data enhances the paleoenvironmental interpretations, and identifies remaining challenges. The paleoclimatic dynamics in the research area at the junction of Atlantic, Mediterranean and continental climatic regimes are discussed. Finally, paleoenvironmental conditions during phases of Upper Paleolithic occupation were equally diverse highlighting anatomically modern humans' ability to adapt to changing paleoenvironments.

A PDF of this thesis can be downloaded from: www.doi.org/10.18154/RWTH-2018-01253

Yan Li

Luminescence dating of transgressions in the Bohai Coast China since the Middle Pleistocene

April 25, 2018

Freie Universität Berlin, Berlin, Germany

Degree: Dr. rer. nat.

Supervisors: Manfred Frechen, Sumiko Tsukamoto

Coastal areas hold major social and economic value. Understanding past coastal evolution is therefore crucial to anticipating future changes which will affect these areas of high significance. The Bohai Sea, situated at the transition zone between the East Eurasian Continent and West Pacific Ocean, is an area particularly sensitive to sea-level changes and sediment inputs. Due to the continuous subsidence of the Bohai basin since the Cenozoic, thick sediment sequences have accumulated progressively on the Bohai Coast, providing a valuable proxy record of climate and environmental evolution. Sedimentary sequences on the Bohai Coast indicate three main transgressive and regressive phases, associated with the regional sea-level change and terrestrial influence since the Middle Pleistocene. The chronology of these transgressions and regressions is however not well constrained, and requires a thorough investigation.

The main objective of this thesis is to establish a reliable chronological framework for the three transgressions identified on the Bohai Coast since the Middle Pleistocene, using Optically Stimulated Luminescence (OSL) dating. A careful validation of different OSL approaches is first conducted. The quartz OSL signal was fully reset for materials from the North Bohai Coast, while the K-feldspar luminescence signals were well bleached for the pre-Holocene deposits, validating the use of this dosimeter to establish a robust chronology of the Bohai sediments. To correct the undesirable signal loss over geological time scale associated with the use of this mineral, the fading correction method based upon the theory of power-law decay of tunnelling is tested. Fading corrected ages in agreement with the reference chronology confirm the validity of this fading correction method. Quartz OSL dating is applied to the coastal core sediments and dune sands from the North Bohai Coast. The quartz and feldspar luminescence chronologies indicate that the earliest transgression occurred ca. 200 ka ago, correlating with the sea-level highstand during Marine Isotope Stage (MIS) 7. Based on the age-depth relation, the second transgression very likely occurred during MIS 5. Both, the radiocarbon dates and the quartz OSL ages show that the transgressive sedimentary facies in association with the rising of the sea-level during MIS 3 is not preserved in the Bohai cores. The last transgression correlates with the Holocene sea-level rise.

Luminescence chronology, in conjunction with the historical records of the shoreline migration, reveals that the sea-level constantly stayed at highstand between ca. 6 and 1 ka in the North Bohai Coast, and then retreated rapidly causing the delta progradation. Thin transgressive deposits, equivalent to an annual sediment increment of 2.7×10^4 m^3/a between 6–1 ka, are explained by the flat relief and insufficient sediment supply. The rapid deltaic progradation, which includes an episodic deposition by multiple flooding events at ca. 700 a, resulted in the dramatic increase of sediment increment (9.1×10^6 m^3/a) over the last millennia. This sudden increase was triggered by both the winter monsoon enhancement and the reduction of plant cover and soil erosion by human activity. On the contrary, a rapid inland sand deposition after the Little Ice Age was most likely related to the Immigrant and Reclamation Policy.

A PDF of this thesis can be downloaded from: http://www.diss.fu-berlin.de/diss/receive/FUDISS_thesis_000000107263

Stefania Cristino de Oliveira

Geomorfologia e cronologia dos depósitos da planície fluvial no Alto Curso do rio Paraná, MS/SP. (Geomorphology and chronology of the fluvial plain deposits in Upper Paraná River Course, MS/SP.)

April 2018

Universidade Estadual Paulista "Júlio de Mesquita Filho", Rio Claro, Brazil

Degree: M.Sc.

Supervisors: Mario Luis Assine, Fabiano do Nascimento Pupim

The knowledge of the geomorphological evolution of the Paraná River fluvial plain in the stretch upstream of the Porto Primavera dam is still precarious, since most of the published works on this fluvial course focused on the stretch downstream of the dam. In this context, the objective of this study was to investigate the succession of geological events responsible for the evolution and current configuration of the river system of the Upper Paraná River, between the Jupiá and Porto Primavera Hydroelectric Plants (between the States of São Paulo and Mato Grosso do Sul). Remote sensing data, sedimentological, geochronological and topobatimetric profiles were used for the development of the research. Four geomorphological compartments were identified and three

of these compartments were dated: Unit 1, raised terrace with circular and semi-circular ponds; Unit 2, intermediate terrace with small ponds and soaked areas (OSL age from 60,5 ± 6,1 kyears); Unit 3, low terrace with preserved paleo canals (OSL age from 39,8 ± 2,8 kyears); and Unit 4, current fluvial plain (OSL age from 8.9 ± 1.6 kyears). The defined geomorphological units were correlated with units of previous works located downstream of the studied area. Unit 1, Unit 3 and Unit 4 are considered extensions of the geomorphological units Taquaruçu, Fazenda Boa Vista and Rio Paraná, respectively. Unit 2 is a compartment with unique morphological characteristics, therefore, not correlated with units presented in previous works. Two zones of *knickpoints* have also been identified that probably occur due to lithological changes in the river thalweg. In addition, in the studied section the Paraná River presents sinuosities that may be related to the sedimentary contribution of the tributaries. Sedimentary records of the deposits of the fluvial plain of the Aguapeí River indicate that this river presented a channel with high energy approximately 8 thousand years ago, when the climate was drier than the present one. Later, about 2,000 years to the present, the region will have similar climatic characteristics to the current ones.

A PDF of this thesis can be downloaded from: http://hdl.handle.net/11449/154032

Marius Pfeifer

Remote Luminescence Dating of Asteroids – A Preliminary Feasibility Study

March 2018

Astrophysical Institute, Göttingen, Germany

Degree: M.Sc.

Supervisors: Dr. Rita Schulz, Prof. Dr. Stefan Dreizler

The purpose of this work is to collect data and results that might be relevant for the development of a procedure for remote OSL dating of asteroids. This work presents a basic summary of each of the major disciplines involved (asteroid research, solid state physics and luminescence dating) up to and including the most recent information available. In addition, it presents an initial assessment of the physical, technical and methodological challenges, and discusses tentative ideas for instrumentation. Lastly, potential approaches for further investigations of certain key aspects are proposed. The hope is that future researchers might be able to use this work as a basis and guideline in follow-up studies.

A PDF of this thesis can be downloaded from: https://www.dropbox.com/s/b3ir5tzoiyfnveh/mthesis_astro.pdf?dl=0

Bibliography

Compiled by Sebastien Huot

From 1st December 2017 to 14th May 2018

Various geological applications

- aeolian

Buckland, C.E., Bailey, R.M., Thomas, D.S.G., 2018. Identifying chronostratigraphic breaks in aeolian sediment profiles using near-surface luminescence dating and changepoint analysis. Quaternary Geochronology 46, 45-58, http://doi.org/10.1016/j.quageo.2018.03.011

Fitzsimmons, K.E., Sprafke, T., Zielhofer, C., Günter, C., Deom, J.-M., Sala, R., Iovita, R., 2018. Loess accumulation in the Tian Shan piedmont: Implications for palaeoenvironmental change in arid Central Asia. Quaternary International 469, 30-43, http://doi.org/10.1016/j.quaint.2016.07.041

Guo, L., Xiong, S., Yang, P., Ye, W., Jin, G., Wu, W., Zhao, H., 2018. Holocene environmental changes in the Horqin desert revealed by OSL dating and δ13C analyses of paleosols. Quaternary International 469, 11-19, http://doi.org/10.1016/j.quaint.2017.06.048

Nash, D.J., Bateman, M.D., Bullard, J.E., Latorre, C., 2018. Late Quaternary coastal evolution and aeolian sedimentation in the tectonically-active southern Atacama Desert, Chile. Palaeogeography, Palaeoclimatology, Palaeoecology 490, 546-562, http://doi.org/10.1016/j.palaeo.2017.11.040

Rowell, A., Thomas, D., Bailey, R., Stone, A., Garzanti, E., Padoan, M., 2018. Controls on sand ramp formation in southern Namibia. Earth Surface Processes and Landforms 43, 150-171, http://doi.org/10.1002/esp.4159

Rowell, A.L.K., Thomas, D.S.G., Bailey, R.M., Holmes, P.J., 2018. Sand ramps as palaeoenvironmental archives: Integrating general principles and regional contexts through reanalysis of the Klipkraal Sands, South Africa. Geomorphology 311, 103-113, http://doi.org/10.1016/j.geomorph.2018.03.021

Sevink, J., van Geel, B., Jansen, B., Wallinga, J., 2018. Early Holocene forest fires, drift sands, and Usselo-type paleosols in the Laarder Wasmeren area near Hilversum, the Netherlands: Implications for the history of sand landscapes and the potential role of Mesolithic land use. CATENA 165, 286-298, http://doi.org/10.1016/j.catena.2018.02.016

Xu, Y., Lai, Z., Chen, T., Gong, S., 2018. Late Quaternary optically stimulated luminescence (OSL) chronology and environmental changes in the Hobq Desert, northern China. Quaternary International 470, 18-25, http://doi.org/10.1016/j.quaint.2017.06.010

- alluvial fan

Lehmkuhl, F., Nottebaum, V., Hülle, D., 2018. Aspects of late Quaternary geomorphological development in the Khangai Mountains and the Gobi Altai Mountains (Mongolia). Geomorphology 312, 24-39, http://doi.org/10.1016/j.geomorph.2018.03.029

- cave

Bacon, A.-M., Antoine, P.-O., Huong, N.T.M., Westaway, K., Tuan, N.A., Duringer, P., Zhao, J.-x., Ponche, J.-L., Dung, S.C., Nghia, T.H., Minh, T.T., Son, P.T., Boyon, M., Thuy, N.T.K., Blin, A., Demeter, F., 2018. A rhinocerotid-dominated megafauna at the MIS6-5 transition: The late Middle Pleistocene Coc Muoi assemblage, Lang Son province, Vietnam. Quaternary Science Reviews 186, 123-141, http://doi.org/10.1016/j.quascirev.2018.02.017

- coastal

Cawthra, H.C., Jacobs, Z., Compton, J.S., Fisher, E.C., Karkanas, P., Marean, C.W., 2018. Depositional and sea-level history from MIS 6 (Termination II) to MIS 3 on the southern continental shelf of South Africa. Quaternary Science Reviews 181, 156-172, http://doi.org/10.1016/j.quascirev.2017.12.002

Ito, K., Tamura, T., Tsukamoto, S., 2017. Post-IR IRSL dating of K-feldspar from last interglacial marine terrace deposits on the Kamikita coastal plain, northeastern Japan. Geochronometria 44, 352-365, http://doi.org/10.1515/geochr-2015-0077

Jiang, T., Liu, X., Yu, T., Hu, Y., 2018. OSL dating of late Holocene coastal sediments and its implication for sea-level eustacy in Hainan Island, Southern China. Quaternary International 468, 24-32, http://doi.org/10.1016/j.quaint.2017.11.039

Kenzler, M., Rother, H., Hüneke, H., Frenzel, P., Strahl, J., Tsukamoto, S., Li, Y., Meng, S., Gallas, J., Frechen, M., 2018. A multi-proxy palaeoenvironmental and geochronological reconstruction of the Saalian-Eemian-Weichselian succession at Klein Klütz Höved, NE Germany. Boreas 47, 114-136, http://doi.org/10.1111/bor.12255

Laermanns, H., Kelterbaum, D., May, S.M., Elashvili, M., Opitz, S., Hülle, D., Rölkens, J., Verheul, J., Riedesel, S., Brückner, H., 2018. Mid- to Late Holocene landscape changes in the Rioni delta area (Kolkheti lowlands, W Georgia). Quaternary International 465, 85-98, http://doi.org/10.1016/j.quaint.2016.12.037

May, S.M., Gelhausen, H., Brill, D., Callow, J.N., Engel, M., Opitz, S., Scheffers, A., Joannes-Boyau, R., Leopold, M., Brückner, H., 2018. Chenier-type ridges in Giralia Bay (Exmouth Gulf, Western Australia) - Processes, chronostratigraphy, and significance for recording past tropical cyclones. Marine Geology 396, 186-204, http://doi.org/10.1016/j.margeo.2017.03.005

Muhs, D.R., Pigati, J.S., Schumann, R.R., Skipp, G.L., Porat, N., DeVogel, S.B., 2018. Quaternary sea-level history and the origin of the northernmost coastal aeolianites in the Americas: Channel Islands National Park, California, USA. Palaeogeography, Palaeoclimatology, Palaeoecology 491, 38-76, http://doi.org/10.1016/j.palaeo.2017.11.042

Muru, M., Rosentau, A., Preusser, F., Plado, J., Sibul, I., Jõeleht, A., Bjursäter, S., Aunap, R., Kriiska, A., 2018. Reconstructing Holocene shore displacement and Stone Age palaeogeography from a foredune sequence on Ruhnu Island, Gulf of Riga, Baltic Sea. Geomorphology 303, 434-445, http://doi.org/10.1016/j.geomorph.2017.12.016

Oliver, T.S.N., Kennedy, D.M., Tamura, T., Murray-Wallace, C.V., Konlechner, T.M., Augustinus, P.C., Woodroffe, C.D., 2018. Interglacial-glacial climatic signatures preserved in a regressive coastal barrier, southeastern Australia. Palaeogeography, Palaeoclimatology, Palaeoecology 501, 124-135, http://doi.org/10.1016/j.palaeo.2018.04.011

Tamura, T., Ito, K., Inoue, T., Sakai, T., 2017. Luminescence dating of Holocene beach-ridge sands on the Yumigahama Peninsula, western Japan. Geochronometria 44, 331-340, http://doi.org/10.1515/geochr-2015-0076

Tamura, T., Nicholas, W.A., Oliver, T.S.N., Brooke, B.P., 2018. Coarse-sand beach ridges at Cowley Beach, north-eastern Australia: Their formative processes and potential as records of tropical cyclone history. Sedimentology 65, 721-744, http://doi.org/10.1111/sed.12402

Taylor, A.K., Benedetti, M.M., Haws, J.A., Lane, C.S., 2018. Mid-Holocene Iberian hydroclimate variability and paleoenvironmental change: molecular and isotopic insights from Praia Rei Cortiço, Portugal. Journal of Quaternary Science 33, 79-92, http://doi.org/10.1002/jqs.3000

Walker, J., Lees, B., Olley, J., Thompson, C., 2018. Dating the Cooloola coastal dunes of South-Eastern Queensland, Australia. Marine Geology 398, 73-85, http://doi.org/10.1016/j.margeo.2017.12.010

Wang, Z., Ryves, D.B., Lei, S., Nian, X., Lv, Y., Tang, L., Wang, L., Wang, J., Chen, J., 2018. Middle Holocene marine flooding and human response in the south Yangtze coastal plain, East China. Quaternary Science Reviews 187, 80-93, http://doi.org/10.1016/j.quascirev.2018.03.001

Werner, V., Baika, K., Fischer, P., Hadler, H., Obrocki, L., Willershäuser, T., Tzigounaki, A., Tsigkou, A., Reicherter, K., Papanikolaou, I., Emde, K., Vött, A., 2018. The sedimentary and geomorphological imprint of the AD 365 tsunami on the coasts of southwestern Crete (Greece) – Examples from Sougia and Palaiochora. Quaternary International 473, 66-90, http://doi.org/10.1016/j.quaint.2017.07.016

- coastal (delta)

Chamberlain, E.L., Törnqvist, T.E., Shen, Z., Mauz, B., Wallinga, J., 2018. Anatomy of Mississippi Delta growth and its implications for coastal restoration. Science Advances 4, http://doi.org/10.1126/sciadv.aar4740

Hijma, M.P., Shen, Z., Törnqvist, T.E., Mauz, B., 2017. Late Holocene evolution of a coupled, mud-dominated delta plain–chenier plain system, coastal Louisiana, USA. Earth Surface Dynamics 5, 689-710, http://doi.org/10.5194/esurf-5-689-2017

Nian, X., Zhang, W., Wang, Z., Sun, Q., Chen, J., Chen, Z., 2018. Optical dating of Holocene sediments from the Yangtze River (Changjiang) Delta, China. Quaternary International 467, 251-263, http://doi.org/10.1016/j.quaint.2018.01.011

Nian, X., Zhang, W., Wang, Z., Sun, Q., Chen, J., Chen, Z., Hutchinson, S.M., 2018. The chronology of a sediment core from incised valley of the Yangtze River delta: Comparative OSL and AMS 14C dating. Marine Geology 395, 320-330, http://doi.org/10.1016/j.margeo.2017.11.008

- colluvial

Kołodyńska-Gawrysiak, R., Poesen, J., Gawrysiak, L., 2018. Assessment of long-term Holocene soil erosion rates in Polish loess areas using sedimentary archives from closed depressions. Earth Surface Processes and Landforms 43, 978-1000, http://doi.org/10.1002/esp.4296

- earthquake (and fault related)

Maestrelli, D., Benvenuti, M., Bonini, M., Carnicelli, S., Piccardi, L., Sani, F., 2018. The structural hinge of a chain-foreland basin: Quaternary activity of the Pede-Apennine Thrust front (Northern Italy). Tectonophysics 723, 117-135, http://doi.org/10.1016/j.tecto.2017.12.006

Yang, H., Chen, J., Porat, N., Li, T., Li, W., Xiao, W., 2017. Coarse versus fine-grain quartz optical dating of the sediments related to the 1985 Ms7.1 Wuqia earthquake, northeastern margin of the Pamir salient, China. Geochronometria 44, 299-306, http://doi.org/10.1515/geochr-2015-0075

Zinke, R., Dolan, J.F., Rhodes, E.J., Van Dissen, R., McGuire, C.P., 2017. Highly Variable Latest Pleistocene-Holocene Incremental Slip Rates on the Awatere Fault at Saxton River, South Island, New Zealand, Revealed by Lidar Mapping and Luminescence Dating. Geophysical Research Letters 44, 11,301-311,310, http://doi.org/10.1002/2017GL075048

- fluvial

Abrahami, R., Huyghe, P., van der Beek, P., Lowick, S., Carcaillet, J., Chakraborty, T., 2018. Late Pleistocene - Holocene development of the Tista megafan (West Bengal, India): 10Be cosmogenic and IRSL age constraints. Quaternary Science Reviews 185, 69-90, http://doi.org/10.1016/j.quascirev.2018.02.001

Bartley, R., Thompson, C., Croke, J., Pietsch, T., Baker, B., Hughes, K., Kinsey-Henderson, A., 2018. Insights into the history and timing of post-European land use disturbance on sedimentation rates in catchments draining to the Great Barrier Reef. Marine Pollution Bulletin 131, Part A, 530-546, http://doi.org/10.1016/j.marpolbul.2018.04.070

Bartz, M., Rixhon, G., Duval, M., King, G.E., Álvarez Posada, C., Parés, J.M., Brückner, H., 2018. Successful combination of electron spin resonance, luminescence and palaeomagnetic dating methods allows reconstruction of the Pleistocene evolution of the lower Moulouya river (NE Morocco). Quaternary Science Reviews 185, 153-171, http://doi.org/10.1016/j.quascirev.2017.11.008

Basu, S., Sanyal, P., Sahoo, K., Chauhan, N., Sarkar, A., Juyal, N., 2018. Variation in monsoonal rainfall sources (Arabian Sea and Bay of Bengal) during the late Quaternary: Implications for regional vegetation and fluvial systems. Palaeogeography, Palaeoclimatology, Palaeoecology 491, 77-91, http://doi.org/10.1016/j.palaeo.2017.11.051

Bufe, A., Burbank, D.W., Liu, L., Bookhagen, B., Qin, J., Chen, J., Li, T., Thompson, J.J.A., Yang, H., 2017. Variations of Lateral Bedrock Erosion Rates Control Planation of Uplifting Folds in the Foreland of the Tian Shan, NW China. Journal of Geophysical Research: Earth Surface 122, 2431-2467, http://doi.org/doi:10.1002/2016JF004099

Cheng, Z., Weng, C., Guo, J., Dai, L., Zhou, Z., 2018. Vegetation responses to late Quaternary climate change in a biodiversity hotspot, the Three Parallel Rivers region in southwestern China. Palaeogeography, Palaeoclimatology, Palaeoecology 491, 10-20, http://doi.org/10.1016/j.palaeo.2017.11.032

Guo, Y., Huang, C.C., Zhou, Y., Pang, J., Zha, X., Fan, L., Mao, P., 2018. Sedimentary record and luminescence chronology of palaeoflood events along the Gold Gorge of the upper Hanjiang River, middle Yangtze River basin, China. Journal of Asian Earth Sciences 156, 96-110, http://doi.org/10.1016/j.jseaes.2017.12.034

Jonell, T.N., Owen, L.A., Carter, A., Schwenniger, J.-L., Clift, P.D., 2017. Quantifying episodic erosion and transient storage on the western margin of the Tibetan Plateau, upper Indus River. Quaternary Research 89, 281-306, http://doi.org/10.1017/qua.2017.92

Li, Y., Tsukamoto, S., Frechen, M., Gabriel, G., 2018. Timing of fluvial sedimentation in the Upper Rhine Graben since the Middle Pleistocene: constraints from quartz and feldspar luminescence dating. Boreas 47, 256-270, http://doi.org/10.1111/bor.12266

Ramírez-Herrera, M.T., Gaidzik, K., Forman, S., Kostoglodov, V., Bürgmann, R., Johnson, C.W., 2018. Relating the long-term and short-term vertical deformation across a transect of the forearc in the central Mexican subduction zone. Geosphere 14, 419-439, http://doi.org/10.1130/GES01446.1

Resmi, M.R., Achyuthan, H., Jaiswal, M.K., 2017. Holocene tectonic uplift using geomorphometric parameters, GIS and OSL dating: Palar River basin, southern peninsular India. Zeitschrift für Geomorphologie 61, 243-265, http://doi.org/10.1127/zfg/2017/0433

Thompson, J.A., Chen, J., Yang, H., Li, T., Bookhagen, B., Burbank, D., 2018. Coarse- versus fine-grain quartz OSL and cosmogenic 10Be dating of deformed fluvial terraces on the northeast Pamir margin, northwest China. Quaternary Geochronology 46, 1-15, http://doi.org/10.1016/j.quageo.2018.01.002

Tóth, O., Sipos, G., Kiss, T., Bartyik, T., 2017. Variation of OSL residual doses in terms of coarse and fine grain modern sediments along the Hungarian section of the Danube. Geochronometria 44, 319-330, http://doi.org/10.1515/geochr-2015-0079

- glacial

Bateman, M.D., Evans, D.J.A., Roberts, D.H., Medialdea, A., Ely, J., Clark, C.D., 2018. The timing and consequences of the blockage of the Humber Gap by the last British–Irish Ice Sheet. Boreas 47, 41-61, http://doi.org/10.1111/bor.12256

Bateman, M.D., Swift, D.A., Piotrowski, J.A., Rhodes, E.J., Damsgaard, A., 2018. Can glacial shearing of sediment reset the signal used for luminescence dating? Geomorphology 306, 90-101, http://doi.org/10.1016/j.geomorph.2018.01.017

Dalton, A.S., Finkelstein, S.A., Barnett, P.J., Väliranta, M., Forman, S.L., 2018. Late Pleistocene chronology, palaeoecology and stratigraphy at a suite of sites along the Albany River, Hudson Bay Lowlands, Canada. Palaeogeography, Palaeoclimatology, Palaeoecology 492, 50-63, http://doi.org/10.1016/j.palaeo.2017.12.011

Ganju, A., Nagar, Y.C., Sharma, L.N., Sharma, S., Juyal, N., 2018. Luminescence chronology and climatic implication of the late quaternary glaciation in the Nubra valley, Karakoram Himalaya, India. Palaeogeography, Palaeoclimatology, Palaeoecology 502, 52-62, http://doi.org/10.1016/j.palaeo.2018.04.022

Gribenski, N., Jansson, K.N., Preusser, F., Harbor, J.M., Stroeven, A.P., Trauerstein, M., Blomdin, R., Heyman, J., Caffee, M.W., Lifton, N.A., Zhang, W., 2018. Re-evaluation of MIS 3 glaciation using cosmogenic radionuclide and single grain luminescence ages, Kanas Valley, Chinese Altai. Journal of Quaternary Science 33, 55-67, http://doi.org/10.1002/jqs.2998

Lang, J., Lauer, T., Winsemann, J., 2018. New age constraints for the Saalian glaciation in northern central Europe: Implications for the extent of ice sheets and related proglacial lake systems. Quaternary Science Reviews 180, 240-259, http://doi.org/10.1016/j.quascirev.2017.11.029

Margold, M., Jansen, J.D., Codilean, A.T., Preusser, F., Gurinov, A.L., Fujioka, T., Fink, D., 2018. Repeated megafloods from glacial Lake Vitim, Siberia, to the Arctic Ocean over the past 60,000 years. Quaternary Science Reviews 187, 41-61, http://doi.org/10.1016/j.quascirev.2018.03.005

Rades, E.F., Fiebig, M., Lüthgens, C., 2018. Luminescence dating of the Rissian type section in southern Germany as a base for correlation. Quaternary International 478, 38-50, http://doi.org/10.1016/j.quaint.2016.07.055

Sacco, D.A., Ward, B.C., Lian, O.B., Maynard, D.E., Geertsema, M., 2017. Quaternary geology of part of the McLeod Lake map area (NTS 093J), central British Columbia: lithostratigraphy, glacial history, and chronology. Canadian Journal of Earth Sciences 54, 1063-1084, http://doi.org/10.1139/cjes-2016-0198

Shukla, T., Mehta, M., Jaiswal, M.K., Srivastava, P., Dobhal, D.P., Nainwal, H.C., Singh, A.K., 2018. Late Quaternary glaciation history of monsoon-dominated Dingad basin, central Himalaya, India. Quaternary Science Reviews 181, 43-64, http://doi.org/10.1016/j.quascirev.2017.11.032

Shulmeister, J., Thackray, G.D., Rittenour, T.M., Hyatt, O.M., 2018. Multiple glacial advances in the Rangitata Valley, South Island, New Zealand, imply roles for Southern Hemisphere westerlies and summer insolation in MIS 3 glacial advances. Quaternary Research 89, 375-393, http://doi.org/10.1017/qua.2017.108

- glacial (lacustrine)

Smith, L.N., Sohbati, R., Buylaert, J.-P., Lian, O.B., Murray, A., Jain, M., 2018. Timing of lake-level changes for a deep last-glacial Lake Missoula: optical dating of the Garden Gulch area, Montana, USA. Quaternary Science Reviews 183, 23-35, http://doi.org/10.1016/j.quascirev.2018.01.009

- lacustrine

Alivernini, M., Lai, Z., Frenzel, P., Fürstenberg, S., Wang, J., Guo, Y., Peng, P., Haberzettl, T., Börner, N., Mischke, S., 2018. Late quaternary lake level changes of Taro Co and neighbouring lakes, southwestern Tibetan Plateau, based on OSL dating and ostracod analysis. Global and Planetary Change 166, 1-18, http://doi.org/10.1016/j.gloplacha.2018.03.016

Hu, G., Yi, C., Zhang, J., Cao, G., Pan, B., Liu, J., Jiang, T., Yi, S., Li, D., Huang, J., 2018. Chronology of a lacustrine core from Lake Linggo Co using a combination of OSL, 14C and 210Pb dating: implications for the dating of lacustrine sediments from the Tibetan Plateau. Boreas 47, 656-670, http://doi.org/doi:10.1111/bor.12291

Kostecki, R., Moska, P., 2017. Baltic Sea Holocene evolution based on OSL and radiocarbon dating: evidence from a sediment core from the Arkona Basin (the southwestern Baltic Sea). Oceanological and Hydrobiological Studies 46, 294, http://doi.org/10.1515/ohs-2017-0031

Smith, L.N., Sohbati, R., Buylaert, J.-P., Lian, O.B., Murray, A., Jain, M., 2018. Timing of lake-level changes for a deep last-glacial Lake Missoula: optical dating of the Garden Gulch area, Montana, USA. Quaternary Science Reviews 183, 23-35, http://doi.org/10.1016/j.quascirev.2018.01.009

Teller, J.T., McGinn, R.A., Rajapara, H.M., Shukla, A.D., Singhvi, A.K., 2018. Optically stimulated luminescence ages from the Lake Agassiz basin in Manitoba. Quaternary Research 89, 478-493, http://doi.org/10.1017/qua.2017.107

Tse, Y.-Y., Li, S.-H., 2017. Optical dating of sediments from manas lake in northwestern china: Paleoenvironmental and neotectonic implications. Geochronometria 44, 175-187, http://doi.org/10.1515/geochr-2015-0063

Wright, E., Kruse, S., Forman, S.L., Harris, M.S., 2017. Millennial Scale Development of a Southeastern United States Spit. Journal of Coastal Research 34, 255-271, http://doi.org/10.2112/JCOASTRES-D-16-00005.1

- loess

Bösken, J., Klasen, N., Zeeden, C., Obreht, I., Marković, S.B., Hambach, U., Lehmkuhl, F., 2017. New luminescence-based geochronology framing the last two glacial cycles at the southern limit of european pleistocene loess in Stalać (Serbia). Geochronometria 44, 150-161, http://doi.org/10.1515/geochr-2015-0062

Chen, J., Yang, T., Matishov, G.G., Velichko, A.A., Zeng, B., He, Y., Shi, P., Fan, Z., Titov, V.V., Borisova, O.K., Timireva, S.N., Konstantinov, E.A., Kononov, Y.M., Kurbanov, R.N., Panin, P.G., Chubarov, I.G., 2018. A luminescence dating study of loess deposits from the Beglitsa section in the Sea of Azov, Russia. Quaternary International 478, 27-37, http://doi.org/10.1016/j.quaint.2017.11.017

Chen, J., Yang, T.-b., Matishov, G.G., Velichko, A.A., Zeng, B., He, Y., Shi, P.-h., 2018. Luminescence chronology and age model application for the upper part of the Chumbur-Kosa loess sequence in the Sea of Azov, Russia. Journal of Mountain Science 15, 504-518, http://doi.org/10.1007/s11629-017-4689-0

Fitzsimmons, K.E., Sprafke, T., Zielhofer, C., Günter, C., Deom, J.-M., Sala, R., Iovita, R., 2018. Loess accumulation in the Tian Shan piedmont: Implications for palaeoenvironmental change in arid Central Asia. Quaternary International 469, 30-43, http://doi.org/10.1016/j.quaint.2016.07.041

Kang, S., Wang, X., Roberts, H.M., Duller, G.A.T., Cheng, P., Lu, Y., An, Z., 2018. Late Holocene anti-phase change in the East Asian summer and winter monsoons. Quaternary Science Reviews 188, 28-36, http://doi.org/10.1016/j.quascirev.2018.03.028

Li, G., Chen, F., Xia, D., Yang, H., Zhang, X., Madsen, D., Oldknow, C., Wei, H., Rao, Z., Qiang, M., 2018. A Tianshan Mountains loess-paleosol sequence indicates anti-phase climatic variations in arid central Asia and in East Asia. Earth and Planetary Science Letters 494, 153-163, http://doi.org/10.1016/j.epsl.2018.04.052

Mayr, C., Matzke-Karasz, R., Stojakowits, P., Lowick, S.E., Zolitschka, B., Heigl, T., Mollath, R., Theuerkauf, M., Weckend, M.O., Bäumler, R., Gregor, H.J., 2017. Palaeoenvironments during MIS 3 and MIS 2 inferred from lacustrine intercalations in the loess–palaeosol sequence at Bobingen (southern Germany). Quaternary Science Journal (Eiszeitalter & Gegenwart) 66, 73-89, http://doi.org/10.5194/egqsj-66-73-2017

Moska, P., Adamiec, G., Jary, Z., Bluszcz, A., 2017. OSL chronostratigraphy for loess deposits from Tyszowce – Poland. Geochronometria 44, 307-318, http://doi.org/10.1515/geochr-2015-0074

Reheis, M.C., Goldstein, H.L., Reynolds, R.L., Forman, S.L., Mahan, S.A., Carrara, P.E., 2017. Late Quaternary loess and soils on uplands in the Canyonlands and Mesa Verde areas, Utah and Colorado. Quaternary Research 89, 718-738, http://doi.org/10.1017/qua.2017.63

Sprafke, T., Fitzsimmons, K.E., Grützner, C., Elliot, A., Marquer, L., Nigmatova, S., 2018. Reevaluation of Late Pleistocene loess profiles at Remizovka (Kazakhstan) indicates the significance of topography in evaluating terrestrial paleoclimate records. Quaternary Research 89, 674-690, http://doi.org/10.1017/qua.2017.103

Stevens, T., Buylaert, J.P., Thiel, C., Újvári, G., Yi, S., Murray, A.S., Frechen, M., Lu, H., 2018. Ice-volume-forced erosion of the Chinese Loess Plateau global Quaternary stratotype site. Nature Communications 9, 983, http://doi.org/10.1038/s41467-018-03329-2

Wang, Y., Chen, T., E, C., An, F., Lai, Z., Zhao, L., Liu, X.-J., 2018. Quartz OSL and K-feldspar post-IR IRSL dating of loess in the Huangshui river valley, northeastern Tibetan plateau. Aeolian Research 33, 23-32, http://doi.org/10.1016/j.aeolia.2018.04.002

Yi, S., Li, X., Han, Z., Lu, H., Liu, J., Wu, J., 2018. High resolution luminescence chronology for Xiashu Loess deposits of Southeastern China. Journal of Asian Earth Sciences 155, 188-197, http://doi.org/10.1016/j.jseaes.2017.11.027

- periglacial

Andrieux, E., Bateman, M.D., Bertran, P., 2018. The chronology of Late Pleistocene thermal contraction cracking derived from sand wedge OSL dating in central and southern France. Global and Planetary Change 162, 84-100, http://doi.org/10.1016/j.gloplacha.2018.01.012

Döhler, S., Terhorst, B., Frechen, M., Zhang, J., Damm, B., 2018. Chronostratigraphic interpretation of intermediate layer formation cycles based on OSL-dates from intercalated slope wash sediments. CATENA 162, 278-290, http://doi.org/10.1016/j.catena.2017.11.003

Wolfe, S.A., Morse, P.D., Neudorf, C.M., Kokelj, S.V., Lian, O.B., O'Neill, H.B., 2018. Contemporary sand wedge development in seasonally frozen ground and paleoenvironmental implications. Geomorphology 308, 215-229, http://doi.org/10.1016/j.geomorph.2018.02.015

- soil

Morris, P., Pillans, B., Williams, F., Spooner, N., Krapf, C., de Souza Kovacs, N., 2018. Combining geochemistry and geochronology of transported regolith to reveal bedrock-hosted mineralization in the arid east Wongatha area of south central Western Australia. Geochemistry: Exploration, Environment, Analysis, http://doi.org/10.1144/geochem2017-056

- surface exposure dating

Lehmann, B., Valla, P.G., King, G.E., Herman, F., 2018. Investigation of OSL surface exposure dating to reconstruct post-LIA glacier fluctuations in the French Alps (Mer de Glace, Mont Blanc massif). Quaternary Geochronology 44, 63-74, http://doi.org/10.1016/j.quageo.2017.12.002

Sohbati, R., Liu, J., Jain, M., Murray, A., Egholm, D., Paris, R., Guralnik, B., 2018. Centennial- to millennial-scale hard rock erosion rates deduced from luminescence-depth profiles. Earth and Planetary Science Letters 493, 218-230, http://doi.org/10.1016/j.epsl.2018.04.017

- thermochronology

Biswas, R.H., Herman, F., King, G.E., Braun, J., 2018. Thermoluminescence of feldspar as a multi-thermochronometer to constrain the temporal variation of rock exhumation in the recent past. Earth and Planetary Science Letters 495, 56-68, http://doi.org/10.1016/j.epsl.2018.04.030

- volcanic

Sears, D.W.G., Sears, H., Sehlke, A., Hughes, S.S., 2018. Induced thermoluminescence as a method for dating recent volcanism: Hawaii County, Hawaii, USA. Journal of Volcanology and Geothermal Research 349, 74-82, http://doi.org/10.1016/j.jvolgeores.2017.09.022

Archaeology applications

Akhilesh, K., Pappu, S., Rajapara, H.M., Gunnell, Y., Shukla, A.D., Singhvi, A.K., 2018. Early Middle Palaeolithic culture in India around 385–172 ka reframes Out of Africa models. Nature 554, 97, http://doi.org/10.1038/nature25444

Álvarez-Alonso, D., de Andrés-Herrero, M., Díez-Herrero, A., Medialdea, A., Rojo-Hernández, J., 2018. Neanderthal settlement in central Iberia: Geo-archaeological research in the Abrigo del Molino site, MIS 3 (Segovia, Iberian Peninsula). Quaternary International 474, 85-97, http://doi.org/10.1016/j.quaint.2016.05.027

Bacon, A.-M., Antoine, P.-O., Huong, N.T.M., Westaway, K., Tuan, N.A., Duringer, P., Zhao, J.-x., Ponche, J.-L., Dung, S.C., Nghia, T.H., Minh, T.T., Son, P.T., Boyon, M., Thuy, N.T.K., Blin, A., Demeter, F., 2018. A rhinocerotid-dominated megafauna at the MIS6-5 transition: The late Middle Pleistocene Coc Muoi assemblage, Lang Son province, Vietnam. Quaternary Science Reviews 186, 123-141, http://doi.org/10.1016/j.quascirev.2018.02.017

Bailiff, I.K., Jankowski, N., Snape, L.M., Gerrard, C.M., Gutiérrez, A., Wilkinson, K.N., 2018. Luminescence dating of qanat technology: prospects for further development. Water History 10, 73-84, http://doi.org/10.1007/s12685-018-0213-x

Finley, J.B., Ideker, C.J., Rittenour, T., 2017. Single-grain optically stimulated luminescence ages of brownware pottery in the Middle Rocky Mountains and the spread of numic ceramic technology. American Antiquity 82, 761-780, http://doi.org/10.1017/aaq.2017.38

Groucutt, H.S., Grün, R., Zalmout, I.A.S., Drake, N.A., Armitage, S.J., Candy, I., Clark-Wilson, R., Louys, J., Breeze, P.S., Duval, M., Buck, L.T., Kivell, T.L., Pomeroy, E., Stephens, N.B., Stock, J.T., Stewart, M., Price, G.J., Kinsley, L., Sung, W.W., Alsharekh, A., Al-Omari, A., Zahir, M., Memesh, A.M., Abdulshakoor, A.J., Al-Masari, A.M., Bahameem, A.A., Al Murayyi, K.M.S., Zahrani, B., Scerri, E.L.M., Petraglia, M.D., 2018. Homo sapiens in Arabia by 85,000 years ago. Nature Ecology & Evolution 2, 800-809, http://doi.org/10.1038/s41559-018-0518-2

Hershkovitz, I., Weber, G.W., Quam, R., Duval, M., Grün, R., Kinsley, L., Ayalon, A., Bar-Matthews, M., Valladas, H., Mercier, N., Arsuaga, J.L., Martinón-Torres, M., Bermúdez de Castro, J.M., Fornai, C., Martín-Francés, L., Sarig, R., May, H., Krenn, V.A., Slon, V., Rodríguez, L., García, R., Lorenzo, C., Carretero, J.M., Frumkin, A., Shahack-Gross, R., Bar-Yosef Mayer, D.E., Cui, Y., Wu, X., Peled, N., Groman-Yaroslavski, I., Weissbrod, L., Yeshurun, R., Tsatskin, A., Zaidner, Y., Weinstein-Evron, M., 2018. The earliest modern humans outside Africa. Science 359, 456-459, http://doi.org/10.1126/science.aap8369

Ingicco, T., van den Bergh, G.D., Jago-on, C., Bahain, J.J., Chacón, M.G., Amano, N., Forestier, H., King, C., Manalo, K., Nomade, S., Pereira, A., Reyes, M.C., Sémah, A.M., Shao, Q., Voinchet, P., Falguères, C., Albers, P.C.H., Lising, M., Lyras, G., Yurnaldi, D., Rochette, P., Bautista, A., de Vos, J., 2018. Earliest known hominin activity in the Philippines by 709 thousand years ago. Nature 557, 233-237, http://doi.org/10.1038/s41586-018-0072-8

Mammadov, S., Gasimov, R., Dadashov, Z., Ahadov, A., 2017. Electron Spin Resonance Dating of Tooth Enamel. International Journal of Research Studies in Science, Engineering and Technology 4, 32-34,

Moropoulou, A., Zacharias, N., Delegou, E.T., Apostolopoulou, M., Palamara, E., Kolaiti, A., 2018. OSL mortar dating to elucidate the construction history of the Tomb Chamber of the Holy Aedicule of the Holy Sepulchre in Jerusalem. Journal of Archaeological Science: Reports 19, 80-91, http://doi.org/10.1016/j.jasrep.2018.02.024

Nerantzis, N., Kazakis, N.A., Sfampa, I.K., Polymeris, G.S., Kitis, G., Tsirliganis, N.C., 2017. An integrated approach to the characterization and dating of furnaces in smelting sites in Macedonia, Greece. Journal of Archaeological Science: Reports 16, 65-72, http://doi.org/10.1016/j.jasrep.2017.09.027

Niang, K., Blinkhorn, J., Ndiaye, M., 2018. The oldest Stone Age occupation of coastal West Africa and its implications for modern human dispersals: New insight from Tiémassas. Quaternary Science Reviews 188, 167-173, http://doi.org/10.1016/j.quascirev.2018.03.022

Nicoll, K., 2018. A revised chronology for Pleistocene paleolakes and Middle Stone Age – Middle Paleolithic cultural activity at Bîr Tirfawi – Bîr Sahara in the Egyptian Sahara. Quaternary International 463, 18-28, http://doi.org/10.1016/j.quaint.2016.08.037

Panzeri, L., Cantù, M., Martini, M., Sibilia, E., 2017. Application of different protocols and age-models in OSL dating of earthen mortars. Geochronometria 44, 341-351, http://doi.org/10.1515/geochr-2015-0072

Parés, J.M., Álvarez, C., Sier, M., Moreno, D., Duval, M., Woodhead, J.D., Ortega, A.I., Campaña, I., Rosell, J., Bermúdez de Castro, J.M., Carbonell, E., 2018. Chronology of the cave interior sediments at Gran Dolina archaeological site, Atapuerca (Spain). Quaternary Science Reviews 186, 1-16, http://doi.org/10.1016/j.quascirev.2018.02.004

Shackelford, L., Demeter, F., Westaway, K., Duringer, P., Ponche, J.-L., Sayavongkhamdy, T., Zhao, J.-X., Barnes, L., Boyon, M., Sichanthongtip, P., Sénégas, F., Patole-Edoumba, E., Coppens, Y., Dumoncel, J., Bacon, A.-M., 2018. Additional evidence for early modern human morphological diversity in Southeast Asia at Tam Pa Ling, Laos. Quaternary International 466, 93-106, http://doi.org/10.1016/j.quaint.2016.12.002

Shipton, C., Roberts, P., Archer, W., Armitage, S.J., Bita, C., Blinkhorn, J., Courtney-Mustaphi, C., Crowther, A., Curtis, R., Errico, F.d., Douka, K., Faulkner, P., Groucutt, H.S., Helm, R., Herries, A.I.R., Jembe, S., Kourampas, N., Lee-Thorp, J., Marchant, R., Mercader, J., Marti, A.P., Prendergast, M.E., Rowson, B.,

Tengeza, A., Tibesasa, R., White, T.S., Petraglia, M.D., Boivin, N., 2018. 78,000-year-old record of Middle and Later stone age innovation in an East African tropical forest. Nature Communications 9, 1832, http://doi.org/10.1038/s41467-018-04057-3

Tengis, S., Saran, S., Munkhbayar, L., Bemmann, J., 2017. Luminescence dating of an ancient walled settlement in Orkhon valley, Mongolia. Proceedings of the Mongolian Academy of Sciences 57, 4-14, http://doi.org/10.5564/pmas.v57i4.918

Thompson, J., C., Mackay, A., Nightingale, S., Wright, D., Choi, J.H., Welling, M., Blackmore, H., Gomani-Chindebvu, E., 2017. Ecological risk, demography and technological complexity in the Late Pleistocene of northern Malawi: implications for geographical patterning in the Middle Stone Age. Journal of Quaternary Science 33, 261-284, http://doi.org/10.1002/jqs.3002

Urbanová, P., Michel, A., Cantin, N., Guibert, P., Lanos, P., Dufresne, P., Garnier, L., 2018. A novel interdisciplinary approach for building archaeology: The integration of mortar "single grain" luminescence dating into archaeological research, the example of Saint Seurin Basilica, Bordeaux. Journal of Archaeological Science: Reports 20, 307-323, http://doi.org/10.1016/j.jasrep.2018.04.009

Villa, P., Pollarolo, L., Conforti, J., Marra, F., Biagioni, C., Degano, I., Lucejko, J.J., Tozzi, C., Pennacchioni, M., Zanchetta, G., Nicosia, C., Martini, M., Sibilia, E., Panzeri, L., 2018. From Neandertals to modern humans: New data on the Uluzzian. PLOS ONE 13, e0196786, http://doi.org/10.1371/journal.pone.0196786

Wang, Z., Ryves, D.B., Lei, S., Nian, X., Lv, Y., Tang, L., Wang, L., Wang, J., Chen, J., 2018. Middle Holocene marine flooding and human response in the south Yangtze coastal plain, East China. Quaternary Science Reviews 187, 80-93, http://doi.org/10.1016/j.quascirev.2018.03.001

Wolf, D., Kolb, T., Alcaraz-Castaño, M., Heinrich, S., Baumgart, P., Calvo, R., Sánchez, J., Ryborz, K., Schäfer, I., Bliedtner, M., Zech, R., Zöller, L., Faust, D., 2018. Climate deteriorations and Neanderthal demise in interior Iberia. Scientific Reports 8, 7048, http://doi.org/10.1038/s41598-018-25343-6

Zielhofer, C., Wellbrock, K., al-Souliman, A.S., von Grafenstein, M., Schneider, B., Fitzsimmons, K., Stele, A., Lauer, T., von Suchodoletz, H., Grottker, M., Gebel, H.G.K., 2018. Climate forcing and shifts in water management on the Northwest Arabian Peninsula (mid-Holocene Rasif wetlands, Saudi Arabia). Quaternary International 473, 120-140, http://doi.org/10.1016/j.quaint.2018.03.001

Zou, G.-N., Shelach, G., Li, X.-Q., Zhao, C., Rui, X., Zhou, L.-P., Zhang, J.-F., 2018. Geochronology and paleoenvironment of the Taoshan site, northeastern China, and archaeological implications. Quaternary International 463, 6-17, http://doi.org/10.1016/j.quaint.2017.06.073

Various ESR applications

Bartz, M., Rixhon, G., Duval, M., King, G.E., Álvarez Posada, C., Parés, J.M., Brückner, H., 2018. Successful combination of electron spin resonance, luminescence and palaeomagnetic dating methods allows reconstruction of the Pleistocene evolution of the lower Moulouya river (NE Morocco). Quaternary Science Reviews 185, 153-171, http://doi.org/10.1016/j.quascirev.2017.11.008

Ekici, G., Sayin, U., Aydin, H., Isik, M., Kapan, S., Demir, A., Engin, B., Delikan, A., Orhan, H., Biyik, R., Ozmen, A., 2018. The importance of pre-annealing treatment for ESR dating of mollusc shells: A key study for İsmil in Konya closed Basin/Turkey. AIP Conference Proceedings 1935, 140002, http://doi.org/10.1063/1.5026005

Groucutt, H.S., Grün, R., Zalmout, I.A.S., Drake, N.A., Armitage, S.J., Candy, I., Clark-Wilson, R., Louys, J., Breeze, P.S., Duval, M., Buck, L.T., Kivell, T.L., Pomeroy, E., Stephens, N.B., Stock, J.T., Stewart, M., Price, G.J., Kinsley, L., Sung, W.W., Alsharekh, A., Al-Omari, A., Zahir, M., Memesh, A.M., Abdulshakoor, A.J., Al-Masari, A.M., Bahameem, A.A., Al Murayyi, K.M.S., Zahrani, B., Scerri, E.L.M., Petraglia, M.D., 2018. Homo sapiens in Arabia by 85,000 years ago. Nature Ecology & Evolution 2, 800-809, http://doi.org/10.1038/s41559-018-0518-2

Hershkovitz, I., Weber, G.W., Quam, R., Duval, M., Grün, R., Kinsley, L., Ayalon, A., Bar-Matthews, M., Valladas, H., Mercier, N., Arsuaga, J.L., Martinón-Torres, M., Bermúdez de Castro, J.M., Fornai, C., Martín-Francés, L., Sarig, R., May, H., Krenn, V.A., Slon, V., Rodríguez, L., García, R., Lorenzo, C., Carretero, J.M., Frumkin, A., Shahack-Gross, R., Bar-Yosef Mayer, D.E., Cui, Y., Wu, X., Peled, N., Groman-Yaroslavski, I., Weissbrod, L., Yeshurun, R., Tsatskin, A., Zaidner, Y., Weinstein-Evron, M., 2018. The earliest modern humans outside Africa. Science 359, 456-459, http://doi.org/10.1126/science.aap8369

Ingicco, T., van den Bergh, G.D., Jago-on, C., Bahain, J.J., Chacón, M.G., Amano, N., Forestier, H., King, C., Manalo, K., Nomade, S., Pereira, A., Reyes, M.C., Sémah, A.M., Shao, Q., Voinchet, P., Falguères, C., Albers, P.C.H., Lising, M., Lyras, G., Yurnaldi, D., Rochette, P., Bautista, A., de Vos, J., 2018. Earliest known hominin activity in the Philippines by 709 thousand years ago. Nature 557, 233-237, http://doi.org/10.1038/s41586-018-0072-8

Joannes-Boyau, R., Duval, M., Bodin, T., 2018. MCDoseE 2.0 A new Markov Chain Monte Carlo program for ESR dose response curve fitting and dose evaluation. Quaternary Geochronology 44, 13-22, http://doi.org/10.1016/j.quageo.2017.11.003

Kinoshita, A., Baffa, O., Mascarenhas, S., 2018. Electron spin resonance (ESR) dose measurement in bone of Hiroshima A-bomb victim. PLOS ONE 13, e0192444, http://doi.org/10.1371/journal.pone.0192444

Mammadov, S., Gasimov, R., Dadashov, Z., Ahadov, A., 2017. Electron Spin Resonance Dating of Tooth Enamel. International Journal of Research Studies in Science, Engineering and Technology 4, 32-34

Parés, J.M., Álvarez, C., Sier, M., Moreno, D., Duval, M., Woodhead, J.D., Ortega, A.I., Campaña, I., Rosell, J., Bermúdez de Castro, J.M., Carbonell, E., 2018. Chronology of the cave interior sediments at Gran Dolina archaeological site, Atapuerca (Spain). Quaternary Science Reviews 186, 1-16, http://doi.org/10.1016/j.quascirev.2018.02.004

Takada, N., Suzuki, A., Ishii, H., Hironaka, K., Hironiwa, T., 2017. Thermoluminescence of coral skeletons: a high-sensitivity proxy of diagenetic alteration of aragonite. Scientific Reports 7, 17969, http://doi.org/10.1038/s41598-017-18269-y

Basic research

Bateman, M.D., Swift, D.A., Piotrowski, J.A., Rhodes, E.J., Damsgaard, A., 2018. Can glacial shearing of sediment reset the signal used for luminescence dating? Geomorphology 306, 90-101, http://doi.org/10.1016/j.geomorph.2018.01.017

Biswas, R.H., Herman, F., King, G.E., Braun, J., 2018. Thermoluminescence of feldspar as a multi-thermochronometer to constrain the temporal variation of rock exhumation in the recent past. Earth and Planetary Science Letters 495, 56-68, http://doi.org/10.1016/j.epsl.2018.04.030

Chithambo, M.L., Niyonzima, P., Kalita, J.M., 2018. Phototransferred thermoluminescence of synthetic quartz: Analysis of illumination-time response curves. Journal of Luminescence 198, 146-154, http://doi.org/10.1016/j.jlumin.2018.02.029

Clark-Balzan, L., Parton, A., Breeze, P.S., Groucutt, H.S., Petraglia, M.D., 2018. Resolving problematic luminescence chronologies for carbonate- and evaporite-rich sediments spanning multiple humid periods in the Jubbah Basin, Saudi Arabia. Quaternary Geochronology 45, 50-73, http://doi.org/10.1016/j.quageo.2017.06.002

Friedrich, J., Fasoli, M., Kreutzer, S., Schmidt, C., 2018. On the dose rate dependence of radiofluorescence signals of natural quartz. Radiation Measurements 111, 19-26, http://doi.org/10.1016/j.radmeas.2018.02.006

Koul, D.K., Soni, A., Datta, D., 2017. Some novel features of post-500°C heating blue stimulated OSL emission of fired natural quartz. Geochronometria 44, 287-298, http://doi.org/10.1515/geochr-2015-0078

Li, B., Jacobs, Z., Roberts, R.G., Li, S.-H., 2018. Single-grain dating of potassium-rich feldspar grains: Towards a global standardised growth curve for the post-IR IRSL signal. Quaternary Geochronology 45, 23-36, http://doi.org/10.1016/j.quageo.2018.02.001

Maghrabi, M., 2018. Dependence of the peak shift, peak height and FWHM of thermoluminescence peaks on the heating rate and trap parameters. Journal of Luminescence 198, 54-58, http://doi.org/10.1016/j.jlumin.2018.02.013

Pagonis, V., Bernier, S., Vieira, F.M.d.S., Steele, S., 2017. The effect of crystal size on tunneling phenomena in luminescent nanodosimetric materials. Nuclear Instruments and Methods in Physics Research Section B: Beam Interactions with Materials and Atoms 412, 198-206, http://doi.org/10.1016/j.nimb.2017.09.016

Prasad, A.K., Poolton, N.R.J., Kook, M., Jain, M., 2017. Optical dating in a new light: A direct, non-destructive probe of trapped electrons. Scientific Reports 7, 12097, http://doi.org/10.1038/s41598-017-10174-8

Riedesel, S., Brill, D., Roberts, H.M., Duller, G.A.T., Garrett, E., Zander, A.M., King, G.E., Tamura, T., Burow, C., Cunningham, A., Seeliger, M., De Batist, M., Heyvaert, V.M.A., Fujiwara, O., Brückner, H., 2018. Single-grain feldspar luminescence chronology of historical extreme wave event deposits recorded in a coastal lowland, Pacific coast of central Japan. Quaternary Geochronology 45, 37-49, http://doi.org/10.1016/j.quageo.2018.01.006

Sawakuchi, A.O., Jain, M., Mineli, T.D., Nogueira, L., Bertassoli, D.J., Häggi, C., Sawakuchi, H.O., Pupim, F.N., Grohmann, C.H., Chiessi, C.M., Zabel, M., Mulitza, S., Mazoca, C.E.M., Cunha, D.F., 2018. Luminescence of quartz and feldspar fingerprints provenance and correlates with the source area denudation in the Amazon River basin. Earth and Planetary Science Letters 492, 152-162, http://doi.org/10.1016/j.epsl.2018.04.006

Takada, N., Suzuki, A., Ishii, H., Hironaka, K., Hironiwa, T., 2017. Thermoluminescence of coral skeletons: a high-sensitivity proxy of diagenetic alteration of aragonite. Scientific Reports 7, 17969, http://doi.org/10.1038/s41598-017-18269-y

Tóth, O., Sipos, G., Kiss, T., Bartyik, T., 2017. Variation of OSL residual doses in terms of coarse and fine grain modern sediments along the Hungarian section of the Danube. Geochronometria 44, 319-330, http://doi.org/10.1515/geochr-2015-0079

Zhang, J., 2018. Behavior of the electron trapping probability change in IRSL dating of K-feldspar: A dose recovery study. Quaternary Geochronology 44, 38-46, http://doi.org/10.1016/j.quageo.2017.12.001

Dose rate issues

Clark-Balzan, L., Parton, A., Breeze, P.S., Groucutt, H.S., Petraglia, M.D., 2018. Resolving problematic luminescence chronologies for carbonate- and evaporite-rich sediments spanning multiple humid periods in the Jubbah Basin, Saudi Arabia. Quaternary Geochronology 45, 50-73, http://doi.org/10.1016/j.quageo.2017.06.002

Jankowski, N.R., Jacobs, Z., 2018. Beta dose variability and its spatial contextualisation in samples used for optical dating: An empirical approach to examining beta microdosimetry. Quaternary Geochronology 44, 23-37, http://doi.org/10.1016/j.quageo.2017.08.005

Urbanová, P., Michel, A., Cantin, N., Guibert, P., Lanos, P., Dufresne, P., Garnier, L., 2018. A novel interdisciplinary approach for building archaeology: The integration of mortar "single grain" luminescence dating into archaeological research, the example of Saint Seurin Basilica, Bordeaux. Journal of Archaeological Science: Reports 20, 307-323, http://doi.org/10.1016/j.jasrep.2018.04.009

Dosimetry

Elashmawy, M., 2018. Study of constraints in using household NaCl salt for retrospective dosimetry. Nuclear Instruments and Methods in Physics Research Section B: Beam Interactions with Materials and Atoms 423, 49-61, http://doi.org/10.1016/j.nimb.2018.03.016

Kalita, J.M., Chithambo, M.L., 2017. A comparative study of the dosimetric features of α-Al2O3:C,Mg and α-Al2O3:C. Radiation Protection Dosimetry 177, 261-271, http://doi.org/10.1093/rpd/ncx039

Kalita, J.M., Chithambo, M.L., 2018. Thermoluminescence of α-Al2O3:C,Mg annealed at 1200 °C. Nuclear Instruments and Methods in Physics Research Section B: Beam Interactions with Materials and Atoms 422, 78-84, http://doi.org/10.1016/j.nimb.2018.03.003

Kinoshita, A., Baffa, O., Mascarenhas, S., 2018. Electron spin resonance (ESR) dose measurement in bone of Hiroshima A-bomb victim. PLOS ONE 13, e0192444, http://doi.org/10.1371/journal.pone.0192444

Musa, Y., Hashim, S., Ghoshal, S.K., Bradley, D.A., Ahmad, N.E., Karim, M.K.A., Hashim, A., Kadir, A.B.A., 2018. General radiographic attributes of optically stimulated luminescence dosimeters: A basic insight. Radiation Physics and Chemistry 147, 1-6, http://doi.org/10.1016/j.radphyschem.2018.01.022

Instruments

Pokorný, P., Novotný, M., Fitl, P., Zuklín, J., Vlček, J., Nikl, J., Marešová, E., Hruška, P., Bulíř, J., Drahokoupil, J., Čerňanský, M., Lančok, J., 2018. Apparatus for measurements of thermal and optical stimulated exo-electron emission and luminescence. Measurement Science and Technology 29, 065902, http://doi.org/10.1088/1361-6501/aabc80

Portable system

Bateman, M.D., Rushby, G., Stein, S., Ashurst, R.A., Stevenson, D., Jones, J.M., Gehrels, W.R., 2018. Can sand dunes be used to study historic storm events? Earth Surface Processes and Landforms 43, 779-790, http://doi.org/10.1002/esp.4255

Castillo, M., Muñoz-Salinas, E., Arce, J.L., Roy, P., 2017. Early Holocene to present landscape dynamics of the tectonic lakes of west-central Mexico. Journal of South American Earth Sciences 80, 120-130, http://doi.org/10.1016/j.jsames.2017.09.024

Muñoz-Salinas, E., Castillo, M., 2018. Assessing conservation practices in Amalacaxco Gorge (Izta-Popo National Park, Central Mexico) using fallout 137CS and Optically Stimulated Luminescence (OSL). Journal of Mountain Science 15, 447-460, http://doi.org/10.1007/s11629-017-4635-1

computer coding

Joannes-Boyau, R., Duval, M., Bodin, T., 2018. MCDoseE 2.0 A new Markov Chain Monte Carlo program for ESR dose response curve fitting and dose evaluation. Quaternary Geochronology 44, 13-22, http://doi.org/10.1016/j.quageo.2017.11.003

Review

Musa, Y., Hashim, S., Ghoshal, S.K., Bradley, D.A., Ahmad, N.E., Karim, M.K.A., Hashim, A., Kadir, A.B.A., 2018. General radiographic attributes of optically stimulated luminescence dosimeters: A basic insight. Radiation Physics and Chemistry 147, 1-6, http://doi.org/10.1016/j.radphyschem.2018.01.022

Thomas, D.S.G., Bailey, R.M., 2017. Is there evidence for global-scale forcing of Southern Hemisphere Quaternary desert dune accumulation? A quantitative method for testing hypotheses of dune system development. Earth Surface Processes and Landforms 42, 2280-2294, http://doi.org/10.1002/esp.4183

Conference Announcements: Central European LED 2018

Central European (German) LED Meeting

Beatenberg, Switzerland
November 23-25, 2018

The Central European (German) LED Meeting will be co-hosted this year by the University of Bern, the University of Lausanne and the Paul Scherrer Institute. In addition to the usual meeting which comprises poster / oral presentations and time for discussion, an optional workshop on "Practical Trapped-Charge Thermo(chrono)metry" will also be offered on November 22nd at the same conference venue.

The conference will take place in Beatenberg, near to Interlaken, which is easily accessed by train, or rail transfer from Bern (1.5 hours), Basel (2.5 hours) or Zürich airport (3 hours). Registration opens in June and the workshop is limited to only 25 places allocated on a first-come first-served basis, so please register early to avoid disappointment. Further details of the conference and workshop can be found on the webpage:

www.dled2018.wordpress.com

We look forward to welcoming you in Switzerland!

Georgina King, Natacha Gribenski, Tobias Sprafke and Pierre Valla
University of Bern

Frédéric Herman and Rabiul Biswas
University of Lausanne

Eduardo Yukihara
Paul Scherrer Institute

Conference Announcements: LAIS 2019

Luminescence in Archaeology International Symposium

Institute of Earth and Environmental Sciences
University of Freiburg, Germany
April 3rd to 6th, 2019

The 4th Luminescence in Archaeology International Symposium will be hosted by the Sedimentary Geology and Quaternary Research Group at the University of Freiburg (Germany). LAIS 2018 continues the series of symposia initiated in Delphi 2009, Lisbon 2012 and Paris 2015. It is an international initiative focusing on the use of luminescence for the dating and analysis of materials in archaeological and geoarchaeological context. In addition, it supports archaeological and archaeometrical communities to further develop and expose luminescence methodology.

Topics

- Advances in luminescence methodology
- Dose rate determination
- Innovative materials
- Application in all fields of archaeological sciences
- (Geo-)Archaeological case studies

Local organiser: F. Preusser
International standing committee: I. Liritzis (Chairman, Rhodes, Greece), N. Zacharias, (Kalamata, Greece), A. Zink (Paris, France), Ana Luisa Rodrigues (Lisbon, Portugal).

Deadlines and costs
Registration: November 1st to December 31st 2018
Late registration: January 1st, 2019 to March 31st 2019
Abstract submission: until December 1st 2018
Abstract confirmation: December 15th 2018
Conference fee: EUR 240,-
Student fee: EUR 160,-
Accompanying persons: EUR 100,-

Conference email: LAIS2019@geologie.uni-freiburg.de
Web page: www.sedimentologie.uni-freiburg.de/lais2019

Ancient TL

ISSN 0735-1348

Aims and Scope

Ancient TL is a journal devoted to Luminescence dating, Electron Spin Resonance (ESR) dating, and related techniques. It aims to publish papers dealing with experimental and theoretical results in this field, with a minimum of delay between submission and publication. Ancient TL also publishes a current bibliography, thesis abstracts, letters, and miscellaneous information, e.g., announcements for meetings.

Frequency

Two issues per annum in June and December

Submission of articles to Ancient TL

Ancient TL has a reviewing system in which direct dialogue is encouraged between reviewers and authors. For instructions to authors and information on how to submit to Ancient TL, please visit the website at:
http://ancienttl.org/TOC1.htm

Journal Enquiries

For enquiries please contact the editor:
Regina DeWitt, Department of Physics, East Carolina University, Howell Science Complex, 1000 E. 5th Street, Greenville, NC 27858, USA; Tel: +252-328-4980; Fax: +252-328-0753 (dewittr@ecu.edu)

Subscriptions to Ancient TL

Ancient TL Vol. 32 No.2 December 2014 was the last issue to be published in print. Past and current issues are available for download free of charge from the Ancient TL website:
http://ancienttl.org/TOC4.htm